Cell Reports
Methods

Article

A widely distributed HIV-1 provirus elimination assay to evaluate latency-reversing agents *in vitro*

Graphical abstract

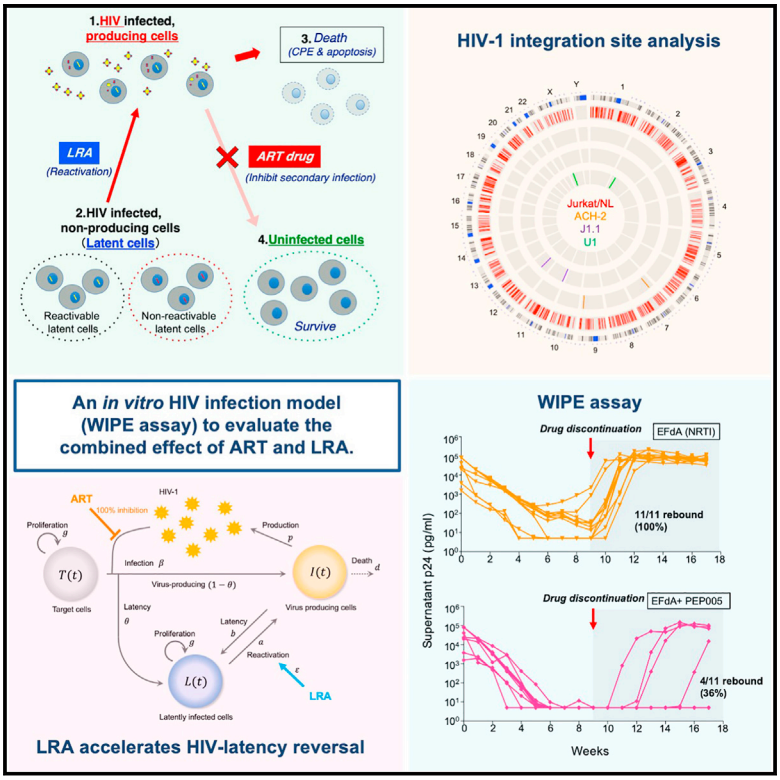

Highlights

- Antiretroviral therapy (ART) cannot eradicate latent reservoir cells in HIV infection
- A cell culture model is established to evaluate drugs for eliminating HIV reservoirs
- Latency-reversing agent (LRA) and ART drug combination inhibits viral re-emergence
- Provides proof-of-concept for "shock and kill" strategy in eliminating HIV reservoirs

Authors

Kouki Matsuda, Saiful Islam, Toru Takada, ..., Shingo Iwami, Yorifumi Satou, Kenji Maeda

Correspondence

kmaeda@ri.ncgm.go.jp (K.M.), y-satou@kumamoto-u.ac.jp (Y.S.)

In brief

Matsuda et al. establish a long-term culture system harboring thousands of different HIV-1-infected cell clones with a distribution of HIV-1 provirus similar to that observed *in vivo*. This model can used to optimize therapeutics against HIV-1 latency and to investigate mechanistic insights into the clonal selection of heterogeneous infected cells.

Matsuda et al., 2021, Cell Reports Methods *1*, 100122
December 20, 2021
https://doi.org/10.1016/j.crmeth.2021.100122

CellPress

Cell Reports Methods

CellPress
OPEN ACCESS

Article

A widely distributed HIV-1 provirus elimination assay to evaluate latency-reversing agents *in vitro*

Kouki Matsuda,[1] Saiful Islam,[2] Toru Takada,[3] Kiyoto Tsuchiya,[4] Benjy Jek Yang Tan,[2] Shin-ichiro Hattori,[1] Hiroo Katsuya,[2,12] Kosaku Kitagawa,[3,13] Kwang Su Kim,[3,13] Misaki Matsuo,[2] Kenji Sugata,[2] Nicole S. Delino,[1] Hiroyuki Gatanaga,[4] Kazuhisa Yoshimura,[2,5,6] Shuzo Matsushita,[2] Hiroaki Mitsuya,[1,7] Shingo Iwami,[3,8,9,10,11,13] Yorifumi Satou,[2,14,*] and Kenji Maeda[1,14,15,*]

[1]National Center for Global Health and Medicine Research Institute, Tokyo, Japan
[2]Joint Research Center for Human Retrovirus Infection, Kumamoto University, Kumamoto, Japan
[3]Department of Biology, Faculty of Sciences, Kyushu University, Fukuoka, Japan
[4]AIDS Clinical Center, National Center for Global Health and Medicine, Tokyo, Japan
[5]AIDS Research Center, National Institute of Infectious Diseases, Tokyo, Japan
[6]Tokyo Metropolitan Institute of Public Health, Tokyo, Japan
[7]HIV and AIDS Malignancy Branch, National Cancer Institute, National Institutes of Health, Bethesda, MD, USA
[8]Institute of Mathematics for Industry, Kyushu University, Fukuoka, Japan
[9]Institute for the Advanced Study of Human Biology (ASHBi), Kyoto University, Kyoto, Japan
[10]NEXT-Ganken Program, Japanese Foundation for Cancer Research (JFCR), Tokyo, Japan
[11]Science Groove Inc., Fukuoka, Japan
[12]Present address: Division of Hematology, Respiratory Medicine, and Oncology, Department of Internal Medicine, Faculty of Medicine, Saga University, Saga, Japan
[13]Present address: interdisciplinary Biology Laboratory (iBLab), Division of Biological Science, Graduate School of Science, Nagoya University, Nagoya, Japan
[14]These authors contributed equally
[15]Lead contact
*Correspondence: y-satou@kumamoto-u.ac.jp (Y.S.), kmaeda@ri.ncgm.go.jp (K.M.)
https://doi.org/10.1016/j.crmeth.2021.100122

MOTIVATION Current therapy regimens for HIV, such as antiretroviral therapy (ART), are mostly efficient in limiting active viral replication. However, these do not act on latent reservoir cells, which are currently one of the major obstacles for eradicating HIV in affected individuals. Several latency-reversing agents (LRAs) that eradicate these reservoir cells are currently being studied, and models for evaluating LRA activity *in vitro* are needed. To address this need, we establish a chronically HIV-1-infected cell culture model called the "widely distributed intact provirus elimination" (WIPE) assay that can recapitulate both ART and LRA effects *in vivo*. The WIPE assay potentially has some advantages over other current models, such as HIV-1 latently infected cell lines, primary cell, or animal models and can be used to optimize therapeutics against HIV-1 latency.

SUMMARY

Persistence of HIV-1 latent reservoir cells during antiretroviral therapy (ART) is a major obstacle for curing HIV-1. Even though latency-reversing agents (LRAs) are under development to reactivate and eradicate latently infected cells, there are few useful models for evaluating LRA activity *in vitro*. Here, we establish a long-term cell culture system called the "widely distributed intact provirus elimination" (WIPE) assay. It harbors thousands of different HIV-1-infected cell clones with a wide distribution of HIV-1 provirus similar to that observed *in vivo*. Mathematical modeling and experimental results from this *in vitro* infection model demonstrates that the addition of an LRA to ART shows a latency-reversing effect and contributes to the eradication of replication-competent HIV-1. The WIPE assay can be used to optimize therapeutics against HIV-1 latency and investigate mechanistic insights into the clonal selection of heterogeneous HIV-1-infected cells.

INTRODUCTION

Advances in antiviral therapy have dramatically improved the therapeutic options available for treating human immunodeficiency virus type 1 (HIV-1) infection. However, even with the potent combined antiretroviral therapy (cART), HIV-1-infected individuals require lifelong antiretroviral therapy (ART) because HIV-1 persists in viral reservoirs *in vivo* (Chun et al., 1997; Finzi et al., 1997; Wong et al., 1997). The "shock and kill" approach—which first activates cells latently infected with HIV-1 (Archin et al., 2012; Deeks, 2012) using HIV-1 latency-reversing agents (LRAs), induces viral production, and eliminates virus-producing cells by immune clearance or viral cytopathic effects (CPE)—is a possible strategy for curing HIV-1 (Bullen et al., 2014; Laird et al., 2015; Matsuda et al., 2019). Previous studies have demonstrated that LRAs were potent in *in vitro* assays but were not necessarily effective *in vivo* because the characteristics of the viral reservoir are quite different between *in vitro* and *in vivo* (Spina et al., 2013). The HIV integration site (IS) significantly impacts the fate of HIV-infected cells, either through vigorous virus production or latent infection. Yet, no *in vitro* system recapitulates the heterogeneity of HIV-infected cells *in vivo* (Cohn et al., 2015; Einkauf et al., 2019; Ho et al., 2013; Liu et al., 2020; Maldarelli et al., 2014; Wagner et al., 2014).

Currently, there are three major model systems that can provide preclinical testing of HIV cure strategies: *in vitro* primary cell or cell line systems, *ex vivo* testing in clinical samples, and *in vivo* animal models. The key determinants to the success of these models is whether they can recapitulate drug effects *in vivo*. In particular, genetic and epigenetic environments are key factors that determine the fate of HIV-1 provirus—either active viral production or viral latency (Einkauf et al., 2019). Currently available *in vitro* models for HIV-1 latency, such as ACH2, J1.1, and U1 cells, carry only one or two proviruses integrated into particular host genomic regions and cannot recapitulate the thousands of different ISs observed *in vivo* (Maldarelli et al., 2014; Wagner et al., 2014). Therefore, LRAs tested in *in vitro* model systems fail to demonstrate responses *ex vivo* (Spina et al., 2013) or *in vivo* (Spivak et al., 2014). Primary cell models recapitulate the diverse ISs (Bosque and Planelles, 2009; Tyagi et al., 2010; Yang et al., 2009), but most cells die in lengthy cultures (Imamichi et al., 2020). *Ex vivo* models using clinical samples from HIV-1-infected individuals may also capitulate the diverse HIV-1 ISs (Bullen et al., 2014). However, the rarity of HIV-1-infected cells in HIV-1-infected individuals (Bruner et al., 2016; Ho et al., 2013) prevents scalable and robust analysis of the impact of LRAs in respect to HIV-1 ISs. Although animal models provide valuable preclinical testing data, the associated costs and resources hinder large-scale screening (Brooks et al., 2003; McBrien et al., 2020; Nixon et al., 2020).

In this study, we aimed to establish an *in vitro* infection model that harbors a much wider variety of HIV-1-infected clones than that of conventional *in vitro* models. Our *in vitro* model, the "widely distributed intact provirus elimination" (WIPE) assay, recapitulates the diverse HIV-1 ISs observed *in vivo*. This cell-line-based *in vitro* system provides not only a robust and scalable system to examine HIV-1 latency reversal, but also a platform to study mechanisms of HIV-1 persistence in respect to the diverse HIV-1 ISs and the host genomic environment.

RESULTS

An *in vitro* model mimicking the distribution of HIV-1 provirus *in vivo*

To establish an HIV-1 chronically infected *in vitro* model with a wide variety of HIV-1-infected clones, several host cell lines were infected with an HIV-1 infectious clone, HIV-1_{NL4-3} or HIV-1_{JRFL}. Cell growth and viral production in the supernatant were monitored twice a week. MT-4 cells infected with HIV-1_{NL4-3} rapidly underwent apoptosis due to vigorous viral production in MT-4 cells, resulting in no live cells remaining after 30 days (data not shown). We analyzed intracellular p24 expression in samples (with cell viability of 60%–70%) on day 30. Jurkat cells infected with HIV-1_{NL4-3} (Jurkat/NL) maintained high levels of viral production (Figure 1A) and cell-associated HIV-1 DNA (Figure 1B). Hut78 cells and MOLT4 cells infected with HIV-1_{NL4-3} also continued to produce HIV-1; however, the viral production and cell-associated HIV-1 DNA decreased on day 30 (Figures 1A and 1B). PM1CCR5 cells infected with HIV-1_{JRFL} (PM1CCR5/JRFL) maintained HIV-1 production and intracellular HIV-1 DNA levels after 30 days of culture; however, the p24 level in the supernatant decreased after 90 days (data not shown). These results indicate that combination(s) of a virus and a cell line with moderate infectivity and moderate cytopathicity may be necessary to establish a chronically HIV-1-infected cell culture model, and Jurkat/NL was the most suitable combination in our study.

Flow cytometry analyses on day 30 revealed four distinct cell populations, including p24-negative live cells, p24-negative dead cells, p24-positive live cells, and p24-positive dead cells (Figure 1C) in the three tested infected cell lines. Based on these results, we focused on Jurkat/NL in this study, since it maintained heterogeneous HIV-1 infectivity for a long period. We confirmed the infectivity of viruses to MT-4 cells produced from Jurkat/NL cells (Figure 1D).

We next analyzed the number of HIV-1-infected clones in the *in vitro* culture model. In principle, each HIV-1-infected clone has a different viral IS, which can be used to distinguish clones. To determine the HIV-1 IS, we performed ligation-mediated polymerase chain reaction (LM-PCR) to detect the junctions between the 3′ long terminal repeat (LTR) of HIV-1 and the flanking host genome sequence (Gillet et al., 2011; Satou et al., 2017). We analyzed genomic DNA extracted from an aliquot of Jurkat/NL cells in the culture and detected approximately 2,933 different ISs, demonstrating the presence of thousands of different infected clones in the culture well (Figure 1E). This was in stark contrast with ACH-2, J1.1, and U1 cell lines, in which only two ISs were detected (Figure 1E). Next, we investigated whether the distribution of HIV-1 proviruses in the *in vitro* system was comparable with that found *in vivo*. We analyzed HIV-1 ISs in peripheral blood mononuclear cells (PBMCs) isolated from HIV-1-infected individuals following the same protocol as that for *in vitro*-cultured cells. We observed several similarities between HIV-1 integration *in vitro* and *in vivo*, i.e., increased integration incidence in certain chromosomes (Figure 1F). First, we found

CellPress
OPEN ACCESS

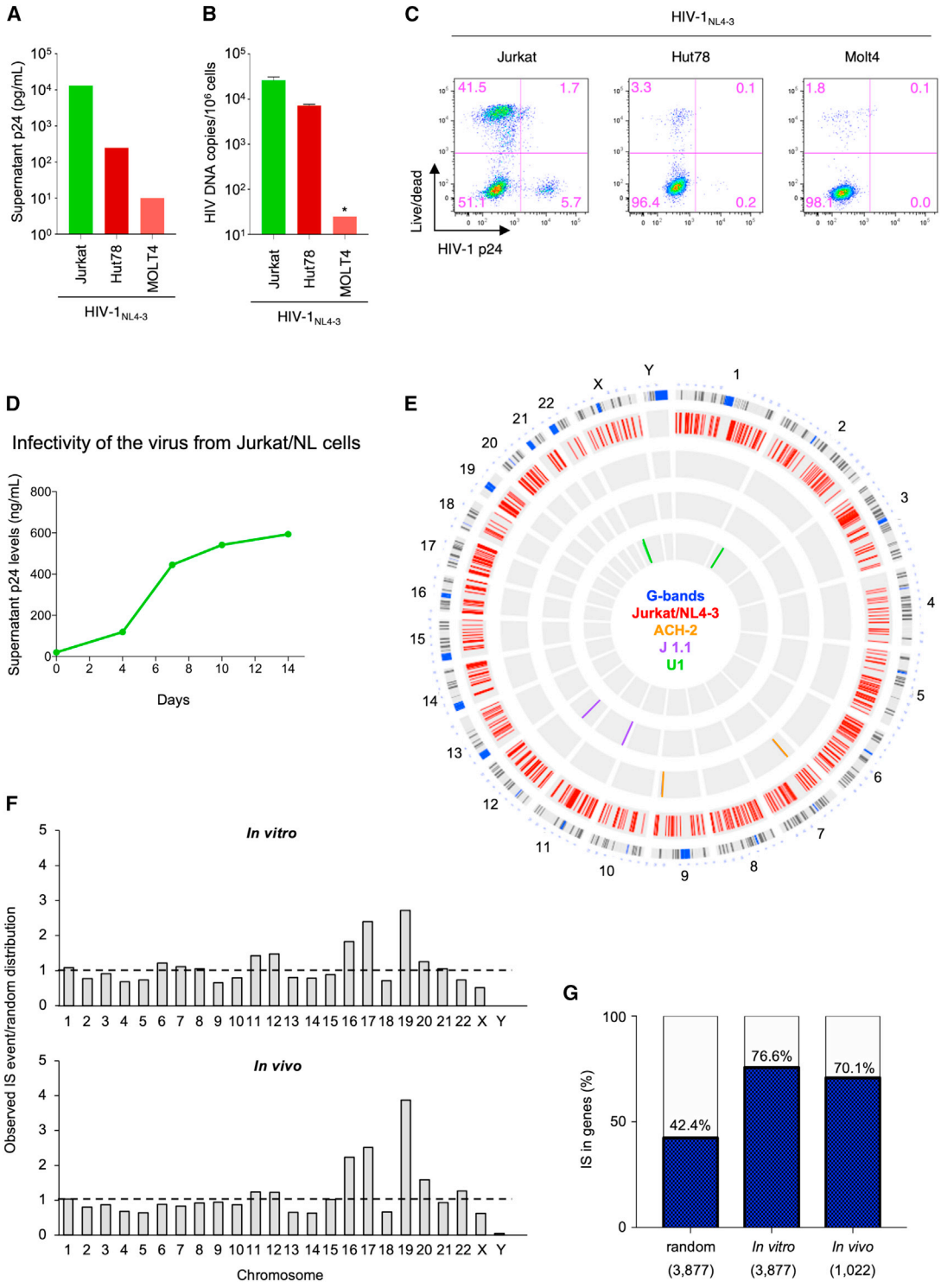

Figure 1. Establishment of an *in vitro* HIV-1 infection model

(A–C) To establish a cell culture model of long-term persistent HIV-1 infection, various T cell lines (Jurkat, Hut78, and MOLT4 cells) were used. HIV-1 production (A) and copies of intracellular HIV-1 DNA (B) on day 30 of each cell line. (C) Co-existence of p24-positive and p24-negative cell populations in HIV-1-infected Jurkat, Hut78, and MOLT4 cell lines. The percentage of intracellular p24-positive cells was analyzed using flow cytometry.

(D) Infectivity of HIV-1_{NL4-3} produced from Jurkat/NL cells. MT4 cells were infected with the virus and cultured for 14 days, and then supernatant p24 levels were measured.

(legend continued on next page)

enrichment of integration in chromatins 16, 17, and 19, similar to that observed *in vivo* (Schroder et al., 2002) (Figure 1F). Second, we observed an enrichment of integration into the host gene bodies (76.6%), similar to those observed *in vivo* (70.1%) (Figure 1G) (Han et al., 2004; Ho et al., 2013; Schroder et al., 2002). Third, we observed that 42.4% of integration is in the same orientation as the host transcription unit, similar to that found *in vivo* (Han et al., 2004; Schroder et al., 2002). These data indicate that our *in vitro* model is far more heterogeneous than conventional latent cell line models for HIV-1 and recapitulates several key aspects about the HIV-1 ISs found *in vivo*.

The WIPE assay recapitulates the effect of LRAs and ARTs in HIV-infected cells

We next evaluated the effect of antiretroviral agents and/or LRAs on various HIV-1-infected clones in the *in vitro* culture (WIPE assay) system. First, we evaluated 11 LRAs, determined their activity in Jurkat/NL cells, and found that PEP005 (ingenol-3-angelate, protein kinase C [PKC] activator) induced HIV-1 production and apoptosis in HIV-1-infected cells at the lowest concentration tested (Figures 2A and 2B). Furthermore, 1 μM SAHA and panobinostat induced strong caspase-3 activation (Figure 2B); however, the same concentration also induced strong cell toxicity in HIV-1-negative cells (data not shown). Hence, we used PEP005 in subsequent experiments. We cultured Jurkat/NL cells in the presence or absence of an antiretroviral drug and/or an LRA (Figure 3A). The assay began with a total of 5×10^4 Jurkat-NL cells in 2 mL culture wells with/without a drug; the cell number reached approximately one million in each well on day 7. The Jurkat-NL cells contain approximately 5×10^4 copies of HIV-1 DNA in 1×10^6 cells (data not shown). The medium in each well was changed every seven days with the same number (5×10^4) of cells with/without a drug. We used the antiretroviral drug EFdA (4′-ethynyl-2-fluoro-2′-deoxyadenosine)/MK-8591/ISL (islatravir), which is a potent nucleoside reverse-transcriptase inhibitor and currently under clinical trials (Nakata et al., 2007). Treatments with EFdA (50 nM), PEP005 (5 nM), or a combination were simultaneously initiated, and supernatant p24 levels were monitored for four months (Figure 3A); time course data from multiple independent experiments are shown in Figure 3B. Treatment with PEP005 alone did not suppress HIV-1 replication during the first nine weeks of cultivation, while EFdA alone successfully decreased viral production in the supernatant to undetectable levels after 4–6 weeks. The combination treatment with EFdA and PEP005 also decreased the amount of HIV-1 in the supernatant to undetectable levels.

We next interrupted the drug treatment in week 9 and observed a significant rebound of viral production in samples treated with EFdA alone (11/11, 100%); however, no rebound was found in 64% (7/11) of samples treated with the combination of EFdA and PEP005 (Figure 3B), which was statistically significant (log rank test, $p < 0.0001$) (Figure 3C). In one representative experiment (experiment 1), viral rebound was observed in cells treated with EFdA only, but not in those treated with both EFdA and PEP005 (Figure 3D). Viral rebound from EFdA + PEP005-treated cells was not detected (in the supernatant or intracellularly; for a total of ∼one million cells in 2 mL culture wells) even after stimulation with tumor necrosis factor alpha (TNF-α) in week 17, confirming lack of replication-competent HIV-1 in the treated sample (Figures 3E and 3F). We also confirmed the HIV-1 mRNA for EFdA-treated and EFdA + PEP005-treated groups, both of which were undetectable when determined with p24 assay (Figure 2C). We found that the supernatant of the EFdA-treated sample, but not of the EFdA + PEP005-treated sample, contained detectable mRNAs and active reverse transcriptase (RT) (Figures 2D and 2E). Combinations with other antiretroviral agents, i.e., darunavir (DRV), a protease inhibitor, and dolutegravir (DTG), an integrase inhibitor, or other LRAs (suberoylanilide hydroxamic acid (SAHA/vorinostat), an histone deacetylase (HDAC) inhibitor or prostratin, a PKC activator) were also tested (Figures 4A–4D). Antiretroviral drugs (DRV, DTG, and EFdA) effectively decreased supernatant HIV-1 levels, whereas most LRAs failed to suppress viral replication when used on their own. However, the combination of an LRA with an antiretroviral drug delayed or inhibited viral rebound after treatment interruption similar to the recent report regarding LRA activity in an *in vivo* model (Borducchi et al., 2018) and clinical trials (Vibholm et al., 2019). Among several drug combinations analyzed in this study, only the combination of EFdA and PEP005 resulted in a significant reduction in viral rebound. Overall, we showed that the WIPE assay is a robust and scalable assay to examine the effect of both ARTs and LRAs.

Combination treatment containing LRAs induces reactivation of latently infected cells and cell apoptosis

The rationale behind using LRAs for an HIV-1 cure is reactivating the latent HIV-1 provirus and inducing cell apoptosis via cytopathic effects or recognition by the host antiviral immunity (Bullen et al., 2014; Hattori et al., 2018). We therefore analyzed whether the reduction in viral rebound observed in this study was indeed mediated by the elimination of latently infected cells. To evaluate such an LRA effect on the elimination of latent cells, each cell population (HIV-1-producing, HIV-1-latently infected, or uninfected) in the culture model was analyzed during the initial phase of the drug treatment. As shown in Figures 5A, 5B, S1A, and S1B, the proportion of latently infected cells did not significantly change in the EFdA-administered group for the first four weeks, but the proportion of the latent cells in the EFdA + LRA-treated

(E) Circos plot depicting viral ISs across the human genome in the Jurkat/NL system and in different cell lines *in vitro*. Each chromosome is presented on the outer circle and is broken down into sequential bins. Blue/black, red, orange, purple, and green bars indicate G-bands (condensed chromosome region by Giemsa staining for karyotyping), Jurkat/NL system, ACH-2, J1.1, and U1, respectively.
(F) Comparison of HIV-1 IS frequency in the individual chromosomes in the *in vitro* model (Jurkat/NL) and *in vivo* in PBMCs from five HIV-1-infected individuals. The y axis depicts the proportion of integration events observed relative to random distribution, with a horizontal dashed black line set at a value of 1.
(G) Relationship between HIV-1 IS and the host genes, *in vitro* and *in vivo*, compared via random distribution. Numbers in parentheses at the bottom of the bars indicate the numbers of unique ISs observed; numbers at the top of the bars indicate the percentage of HIV-1 proviruses integrated within the host genes in each group. Asterisk (*) represents below detection limit.

CellPress
OPEN ACCESS

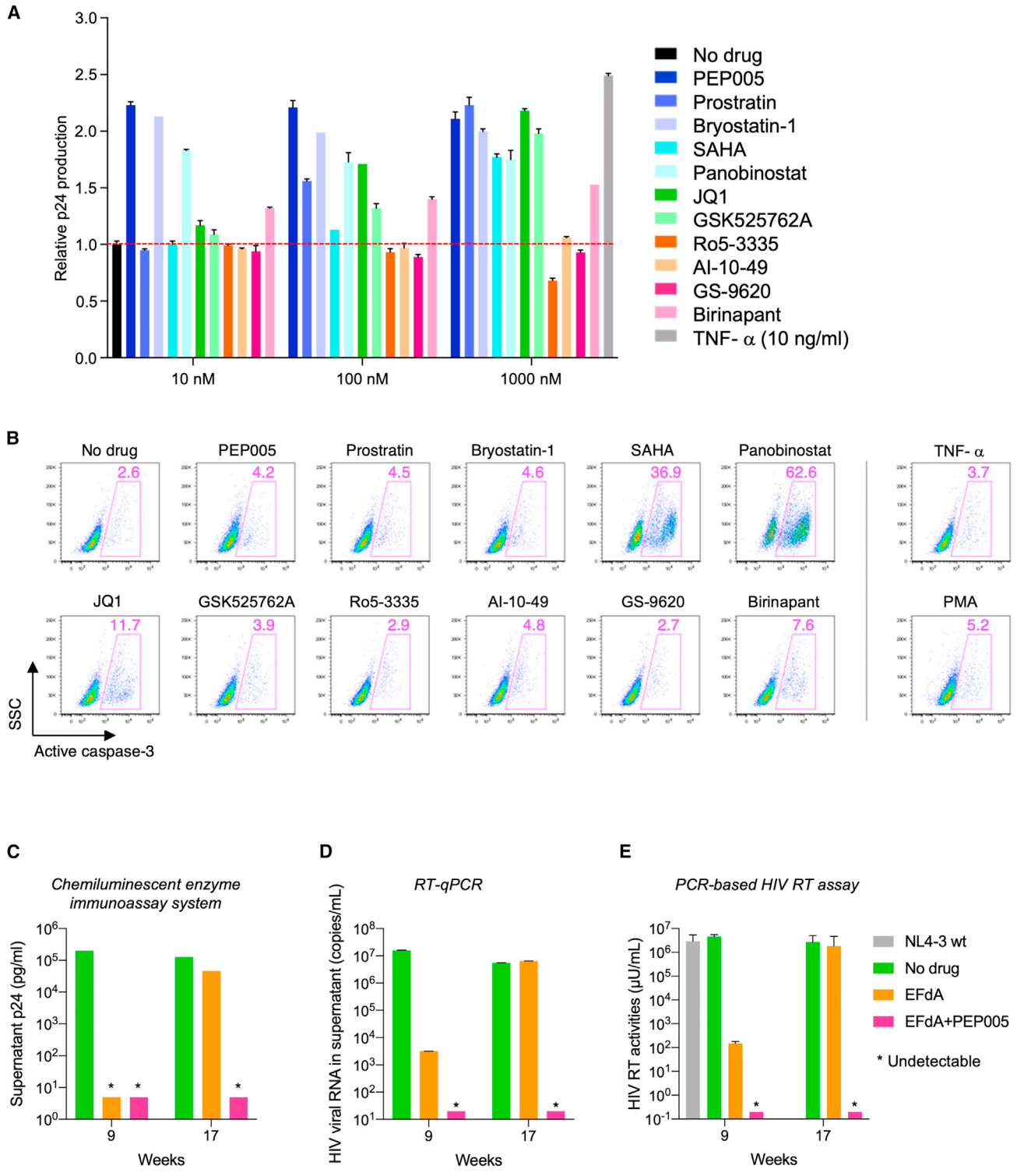

Figure 2. Effects of a drug on HIV-1-infected cells and in the supernatant virus

Efficacy of LRAs in inducing HIV-1 production or caspase-3 activation in Jurkat/NL cells. Cells were treated with a drug (1 μM) for 24 h, and the changes in supernatant p24 values (A) or percentage of active forms of caspase-3 expression (B) were examined. Changes in the supernatant viral titers on weeks 9 and 17 when determined in p24 values (C), HIV-1 RNA copies (D), and RT enzyme activity (E). Asterisk (*) represents below detection limit.

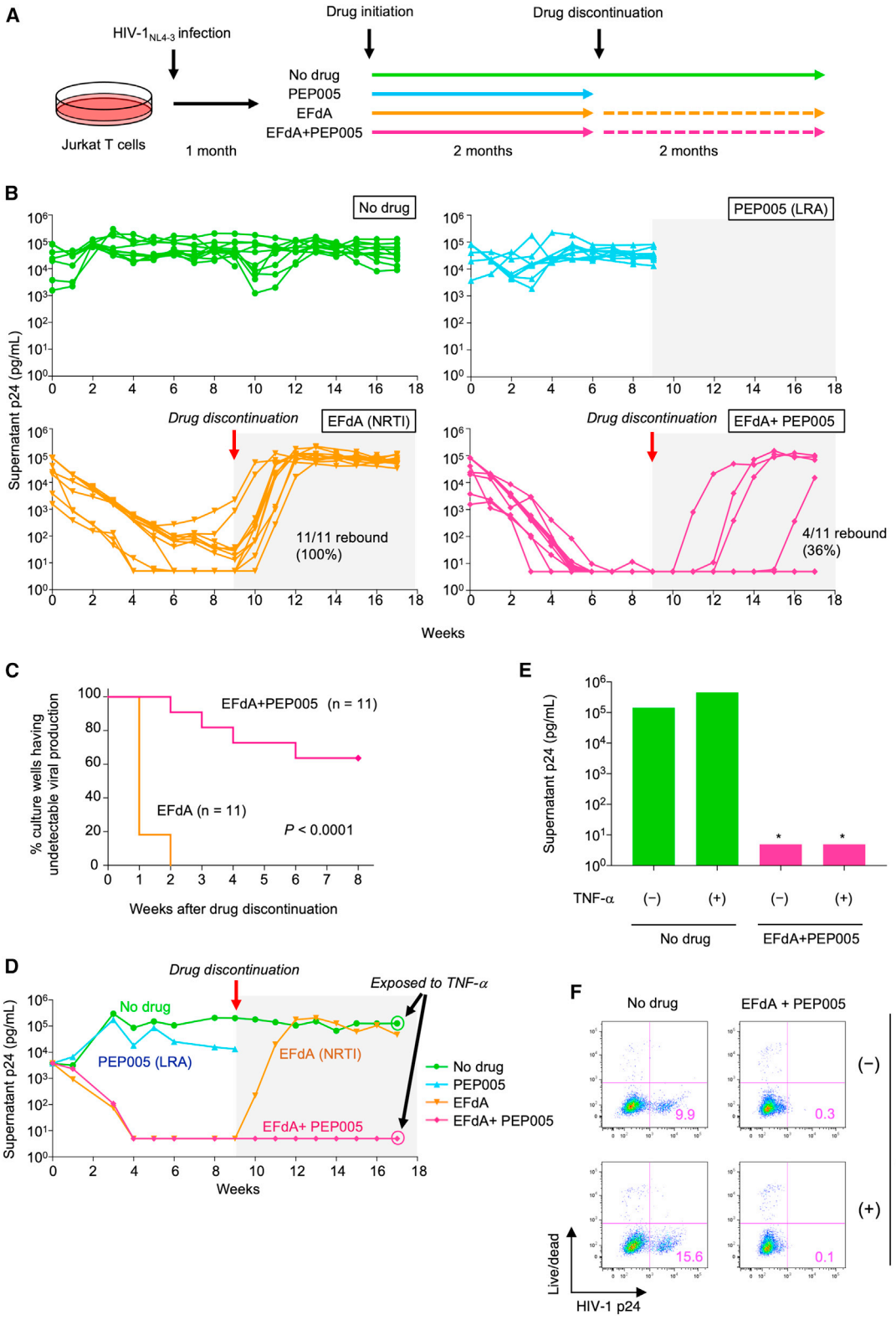

(legend on next page)

group rapidly decreased (Figure 5B), presumably because LRA shortened the time required for the activation of latently infected cells (Figure 6B), thereby rapidly inducing apoptosis.

Since antiviral cytotoxic T lymphocytes (CTLs) and antibodies are absent in the Jurkat/NL system, latent HIV-1-infected cells reactivated by PEP005 would have been eliminated mainly by viral cytopathicity or cell apoptosis (Figure 2B) (Hattori et al., 2018; Kim et al., 2018). To analyze the relationship between viral protein production and cell apoptosis, we examined intracellular HIV-1 p24 and cell apoptosis using flow cytometry during the early phase of drug treatment. We observed an increase in p24 protein expression in cells treated with PEP005 (±EFdA) at 6 h following drug treatment initiation (Figure 5C), which was followed by an increase in annexin V expression (Figure 5D). The number of intracellular $p24^{+}$ cells decreased in EFdA- or EFdA + PEP005-treated cell populations, and these cells constituted less than 2.5% of the total population by week 2 (data not shown). On week 4, we analyzed caspase-3 levels in these cells and found that caspase-3 expression was much higher in $p24^{+}$ cells, especially in the EFdA + PEP005-treated cells, than in $p24^{-}$ cells (Figure 5E). These observations suggest that PEP005 functions as an LRA, inducing apoptosis in cells latently infected with HIV-1 and facilitating the elimination of HIV-1 replicable cells *in vitro*. The proportion of the full-length-type provirus among total proviruses in EFdA alone or EFdA + PEP005-treated cells also decreased but was nonetheless more than 50% after the initial three-week treatment (Figure 5F), suggesting that more than half of all proviruses were thought to be replication-competent at this time point. Collectively, these data indicate that the elimination of HIV-1 producible cells achieved in this study was at least partially due to the reactivation of latent HIV-1 reservoirs.

Next, we investigated if there would be latent clones in the Jurkat/NL system by infecting Jurkat-LTR-green fluorescent protein (GFP) cells (Jurkat cells stably transfected with a plasmid containing the GFP reporter gene driven by the HIV-1 promoter LTR) with $HIV\text{-}1_{NL4\text{-}3}$, in which GFP expression is dependent on the presence of exogenous viral protein Tat. We sorted and stimulated the GFP-negative cell fraction with TNF-α, which increased proviral transcription in this fraction (Figures 5G and 5H), indicating the presence of latently infected cells in the Jurkat/NL system. The percentage of such latently infected cells was approximately 1% in this assay (Figure 5I).

Quantifying reactivation dynamics of latent HIV-1 reservoirs reveals significant reduction of the time until reactivation

To analyze how the addition of LRAs affects the kinetics of HIV-1 replication in the WIPE assay, we developed a mathematical model describing HIV-1 infection dynamics with antiviral drugs. Then, to assess the variability of kinetic parameters and model predictions, we performed Bayesian estimation for the whole dataset using Markov chain Monte Carlo (MCMC) sampling. The typical behavior of the model using these best-fit parameter estimates, along with the data, is shown in Figure 6A, which indicates that the mathematical model has described the WIPE assay data well. The shadowed regions correspond to 95% posterior predictive intervals, the solid lines give the best-fit solution (mean) for the mathematical model, and the colored dots show the experimental datasets. Note that our mathematical model does not account for defective proviral DNA, but our experimental measurement included the defective provirus. Since most of proviral DNA were defective in EFdA + PEP005-treated cells (see Figures 7B and 7C in the next section), our mathematical model, which predicts only intact proviral DNA, underestimated the normalized proviral load but predicted the proviral load in EFdA-treated cells well since most proviral DNA were intact.

To evaluate whether PEP005 treatment induced the reactivation of latent HIV-1 reservoirs in the WIPE assay, we applied our mathematical model to time course experimental data. With estimated distributions of parameters a and ε, we calculated the distribution for the time until reactivation without and with PEP005 treatment ($1/a$ and $1/\varepsilon a$, respectively) (Figure 6B). Comparing these lengths without and with PEP005 treatment showed a significant difference (29.1 days; 95% confidence interval (CI): 15.9–52.1 days and 13.9 days; 95% CI: 7.85–24.3 days, respectively) ($p = 2.59 \times 10^{-4}$ by repeated bootstrap t test). These estimates indicated that PEP005 treatment induced the reactivation in the WIPE assay and significantly reduced the time until reactivation (52.2% reduction on average).

Long-term LRA + ART preferentially selects infected clones with defective HIV-1 proviruses

To elucidate the possible mechanism(s) underlying the reduction in viral rebound *in vitro,* we quantitatively and qualitatively analyzed HIV-1 proviruses during the time course of treatment. We analyzed cell-associated HIV-1 DNA loads in one representative experiment (experiment 6; Figure S2A) and found that the HIV-1 DNA load was markedly decreased in samples treated with EFdA alone (Figure 7A). The addition of PEP005 to EFdA further decreased the HIV-1 DNA load (Figure 7A). After drug discontinuation, the HIV-1 DNA load increased in the sample treated with EFdA alone, but not in the sample treated with both drugs (Figure 7A). We characterized the structure of the HIV-1 proviral genome by nearly full-length PCR, using a single copy of the HIV-1 genome as a template (Imamichi et al., 2016). We observed an increased proportion of a defective

Figure 3. Effect of drug treatments on viral persistence in the *in vitro* infection model

(A) Assay overview. Schematic representation of the assay protocol involving the $HIV\text{-}1_{NL4\text{-}3}$-infected cell culture model (Jurkat/NL cells).

(B) Changes in supernatant p24 levels without drugs, with 5 nM PEP005 or 50 nM EFdA, or with a combination of 50 nM EFdA and 5 nM PEP005 (n = 11, 9, 11, and 11, respectively). Drug treatment was terminated on week 9, but analysis continued for an additional 8 weeks.

(C) Log rank test comparison of the percentage of non-recurrence in the EFdA single treatment and the combination treatment.

(D) Changes in supernatant p24 levels in a representative experiment (experiment 1) from experiments shown in Figure 3B.

(E and F) Assessment of the viral rebound in Jurkat/NL cells after drug discontinuation. Cells treated with drugs or untreated cells were stimulated with TNF-α (10 ng/mL) in week 17, and supernatant p24 (E) and intracellular p24 levels (F) were analyzed on day 6 after stimulation. Asterisk (*) denotes below detection limit.

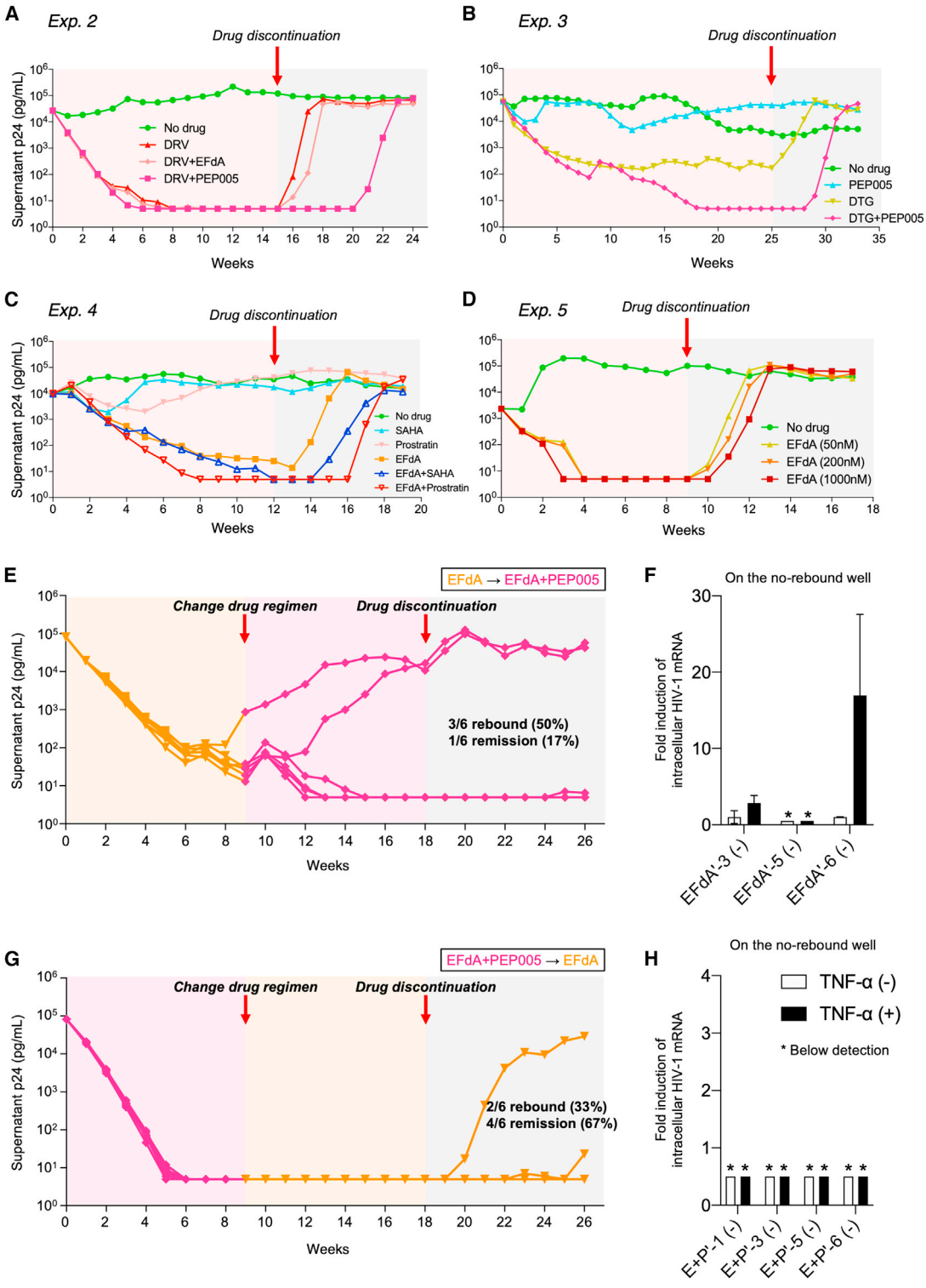

Figure 4. Effect of various combinations of antiretroviral drugs and LRAs on viral persistence

(A–C) Changes in HIV-1 production under treatment with 5 nM PEP005, 50 nM EFdA, and/or 500 nM DRV (protease inhibitor) (A); 5 nM PEP005 and/or 50 nM DTG (integrase inhibitor) (B); 100 nM EFdA, 500 nM SAHA (HDAC inhibitor), and/or 500 nM prostratin (PKC activator) (C).

(D) EFdA at different concentrations (50 nM, 200 nM, or 1 μM) was examined. A higher concentration of EFdA (200 nM and 1 μM) slightly delayed the recurrence of supernatant viruses post treatment interruption.

(legend continued on next page)

HIV-1 genome after EFdA treatment at 9 weeks, possibly due to preferential elimination of intact, replication-competent proviruses (Figures 7B and 7C). But, after drug discontinuation of EFdA treatment at 17 weeks, intact HIV-1 proviruses emerged again, suggesting new rounds of infection from latently infected cells harboring replication-competent HIV-1 (Figures 7B and 7C). Combination of ART (EFdA) and LRA (PEP005) eliminated intact proviruses (Figures 7B and 7C), suggesting that LRA has reactivated all cells harboring replication-competent HIV and exposed them for viral cytopathic effect and cell death. All proviruses detected in the sample after a combined EFdA and PEP005 treatment were defective at 17 weeks after drug treatment initiation (Figures 7B and 7C). Accumulation of defective proviruses during ART has previously been reported (Ho et al., 2013; Imamichi et al., 2016), which was also confirmed in this study. We analyzed peripheral blood samples of HIV-1-carrying individuals (Table S1, panel A) with nearly full-length, single-genome PCR. Before the initiation of cART, 25%–42% proviruses in PBMCs from HIV-1-infected individuals were defective, and the ratio increased to 83%–100% after successful cART (treatment duration of at least 7 years) (Figures 7D, S3A, and S3B). The data suggest that our WIPE assay recapitulated the accumulation of defective proviruses *in vivo* caused by a preferential selection of defective and/or replication-incompetent proviruses during long-term antiretroviral treatment.

We also analyzed HIV-1 proviruses in experiment 1 (Figure 3D) and similarly found that the HIV-1 DNA load was markedly decreased in samples treated with EFdA alone or EFdA together with PEP005 (Figure 7E). Nearly full-length HIV-1 PCR and sequencing analysis (Imamichi et al., 2016) revealed that all remaining proviruses under combination treatment did not contain any critical mutations or deletions in the regions coding for viral proteins (Figure 7F). However, these cells did not transcribe HIV-1 mRNA after TNF-α stimulation (Figure S2B), hence we hypothesized possible deletions or mutations in the provirus outside the primer-binding sites of the nearly full-length HIV-1 PCR. To test this hypothesis, we analyzed the whole sequence of the 5′ LTR. First, we determined HIV-1 ISs using LM-PCR (Satou et al., 2017) with PCR primers to amplify the junction between the host and the viral genome. Since we can obtain the information of clonal abundance of each HIV-1-infected clone using LM-PCR (Maldarelli et al., 2014; Satou et al., 2017; Wagner et al., 2014), we incidentally found that one infected clone was significantly expanded (Figure 7G). A part of the 5′ LTR, including the transcription start site, in the expanded clone was deleted (Figures 7H and S2C), which explains the observed lack of virus rebound. Interestingly, *NSD3* gene is known as a cancer-related gene targeted by HIV-1 integration in an HIV-1-infected individual under cART (Maldarelli et al., 2014).

In this study, we observed the following mechanisms underlying successful elimination of HIV-1 producible cells *in vitro*: (1) large deletion(s) in viral protein-coding regions; (2) critical mutation(s), such as nonsense mutations and frameshift mutations (Figures S4A–S4D), in the viral coding sequence; and (3) abnormalities in HIV-1 proviral transcription (a schematic diagram is shown in Figure S5) (Bruner et al., 2016; Imamichi et al., 2016; Sanchez et al., 1997). A long-term antiretroviral treatment in HIV-1-infected individuals reduces the numbers of replication-incompetent proviruses and increases the proportion of defective HIV-1 proviruses in a previous study (Bruner et al., 2016) and in this study (Figures 7D and S3). However, it is likely that a minor cell population with replication-competent HIV-1 proviruses persists during the long period of cART, maintaining the ability to reverse HIV-1 latency (Ho et al., 2013; Matsuda et al., 2019). We demonstrated that the addition of an LRA to an antiretroviral drug could accelerate the elimination of cells infected with replication-competent HIV-1 proviruses that exist, even as a minor population, in Jurkat/NL cells.

DISCUSSION

The usage of LRAs aims to reactivate latent proviruses to induce production of viral antigens and/or HIV-1 virions. A number of studies have demonstrated that recently developed small-molecule compounds have the ability to reverse latently HIV-1-infected cells (Bullen et al., 2014; Laird et al., 2015). However, Battivelli et al. reported that LRAs could reactivate only a part of infected cells with latent proviruses using their *in vitro* model, demonstrating a wide variation in drug susceptibility to LRAs among different HIV-1-infected clones. The genetic and epigenetic environments of integrated proviruses play a role in such different drug susceptibility. HIV-1 preferentially integrates into the genomic region with active transcription, resulting in a high proportion of HIV-1 integration within the host gene body (Schroder et al., 2002) (Figure 1G). Transcriptional interference between the host genes and integrated proviruses is another factor that affects proviral transcription (Han et al., 2008; Lenasi et al., 2008). A recent study reported a higher proportion of intact proviruses integrated in the opposite orientation relative to the host genes in $CD4^+$ T cells of HIV-1-infected individuals under cART (Einkauf et al., 2019). In addition, the epigenetic status of the integrated provirus is associated with accessibility of transcription factors that drive promoter activity of the 5′ LTR. These findings indicate that susceptibility to LRAs among different HIV-1 clones is variable depending on the genetic and epigenetic environments of integrated proviruses. Thus, we must develop drug combinations that are effective to reactivate a wide variety of HIV-1 proviruses to eliminate cells with replication-competent provirus. However, currently available *in vitro* latent models to evaluate LRA activity carry only one or two integrated HIV-1 proviruses (Figure 1E). Thus, a compound can potently reactivate a specific HIV-1 provirus in a latent cell line, but may not do so for other clones. To our knowledge, this is the first report describing an *in vitro* model available for evaluating the long-term effects of LRAs on a variety of HIV-1 clones. Here, we show that the WIPE assay could be used to analyze the effect of drug treatment on

(E–H) Effect of different drug treatment protocols in the WIPE assay. (E) Changes in supernatant p24 levels with 50 nM EFdA for 9 weeks and then FFdA + PEP005 (5 nM) for an additional 9 weeks (n = 6). (F) Analysis of HIV-1 mRNA transcripts after TNF-α stimulation in cells without viral rebound on week 26 (three samples). (G) Changes in supernatant p24 levels with EFdA + PEP005 followed by the EFdA treatment for 9 weeks. (H) Analysis of HIV-1 mRNA transcripts after TNF-α stimulation in cells without viral rebound on week 26 (four samples). Asterisk (*) represents below detection limit.

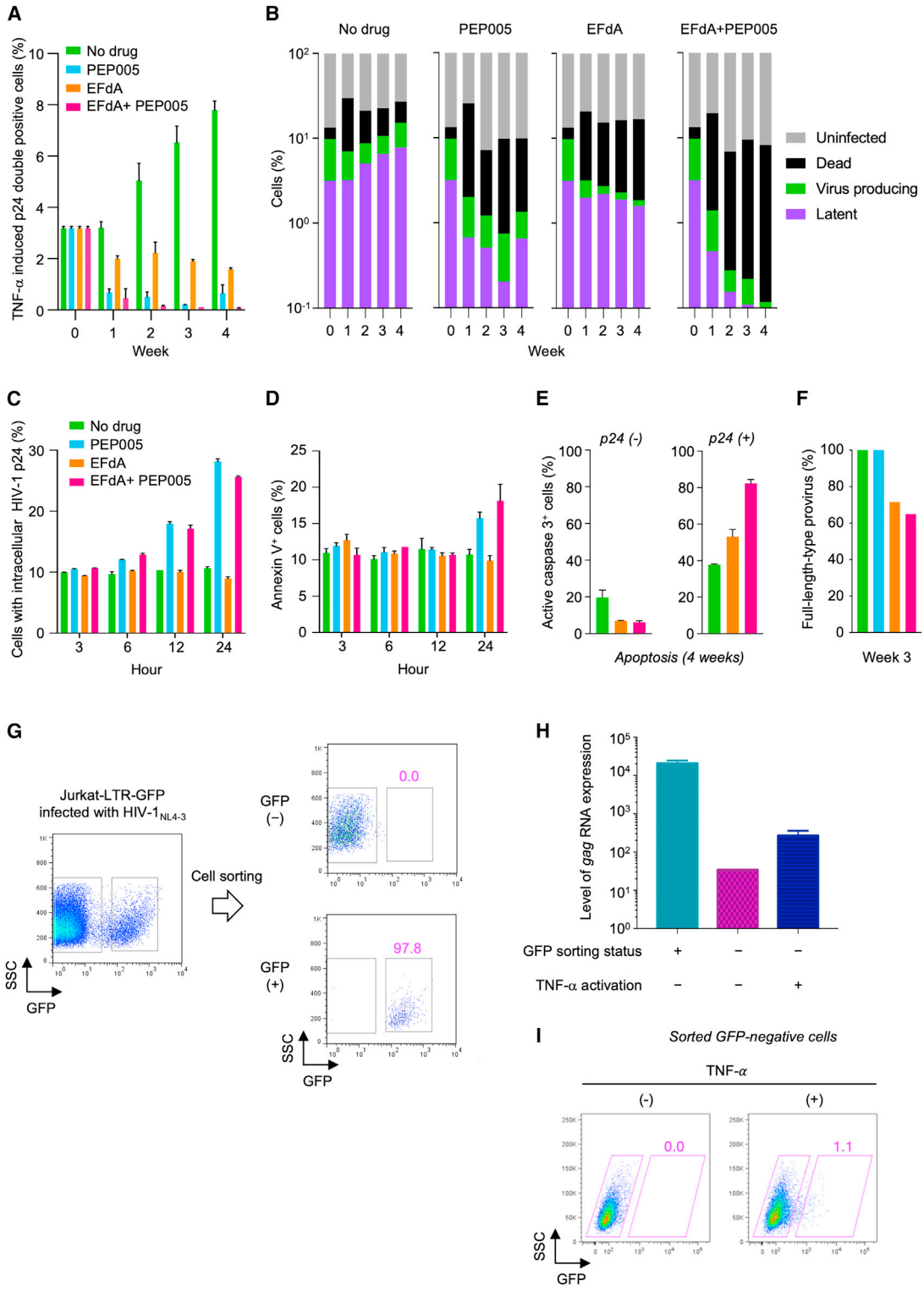

Figure 5. Proof-of-concept of the "shock and kill" strategy of the WIPE assay

(A) Cell samples from the WIPE assay (weeks 0, 1, 2, 3, and 4) were stimulated with TNF-α (for 24 h), and the increased percentages of p24 double-positive cells, which are considered to be an HIV-1 latent cell population, are shown.

(B) Changes in the percentages of each population (uninfected, dead, virus-producing, and latent) in cells from the WIPE assay (on weeks 0–4) are summarized. The ratios of dead cells in the assay were analyzed using cell viability dye (Ghost Dye).

(legend continued on next page)

several thousand different clones with a similar distribution of HIV-1 proviruses as observed *in vivo* (Figures 1F and 1G). The WIPE assay, along with an in-depth characterization of the HIV-1 provirus, would provide further insights into the underlying mechanism of HIV-1 latency, which cannot be obtained using conventional latent cell lines. Further studies using the WIPE assay may also provide mechanistic insights on molecular targeting not only by LRAs but also by novel strategies; for example, the "block-and-lock" strategy was recently proposed, in which particular agents lock the HIV-1 promoter in a deep latency state to prevent viral reactivation (Darcis et al., 2017; Kessing et al., 2017).

We utilized the WIPE assay to evaluate the reduction and eradication of replication-competent HIV-1-DNA after a combination therapy of existing ART drug(s) with LRA(s). In the Jurkat/NL system, there is a continuous and dynamic viral infection, including *de novo* infection, cell apoptosis triggered by viral production, replication of uninfected cells, and generation of latently infected cells. ART drugs inhibit *de novo* infection of uninfected cells by an infected one, while LRAs activate latently infected cells and induce reactivation of viral antigen expression. As shown in Figures 4A–4D, multiple LRAs and ART drugs showed activity in the WIPE assay, and we found that PEP005 was the most potent in eliminating HIV-1-infected cells. However, our preliminary data showed that the potency of PEP005 in a primary cell model was not as potent. Thus, the detailed potency profile of each LRA may be different depending on cells or other circumstance. Since there are no antiviral CTLs and antibodies in the WIPE assay, elimination of reactivated cells is mostly due to viral cytopathicity or apoptosis of the reactivated cells. Although productive HIV-1 replication can be cytotoxic for the cells, HIV-1 production does not always kill these cells. However, under certain conditions, such as p53 activation, Bcl2 inhibition and PKC activation can modulate the condition of the latent-infected cells to turn into apoptosis-sensitive cells (Badley et al., 2013). Notably, we recently reported that some LRAs, such as PEP005, strongly induce the upregulation of active caspase-3, resulting in enhanced apoptosis (Hattori et al., 2018), which may explain why the addition of an LRA successfully accelerated the elimination of latently HIV-1-infected cells in the WIPE assay even in the absence of the host immune system. Our quantitative analysis with the mathematical model revealed that PEP005 treatment reduced 52.2% of the time until reactivation in WIPE assay (Figure 6B).

When HIV-1 cure strategies become available, LRAs can be administered to patients on ART in whom viral replication has been suppressed for a long period of time. To model this scenario, we conducted experiments in which LRA(s) and ART drug(s) were added at different time points during treatment (e.g., treated with an ART drug first and then LRA was added). Figure 4E shows the experiment in which the cells were first treated with EFdA for nine weeks and then an LRA (PEP005) was added. On week 9, following PEP005 addition to EFdA, elevation of the supernatant virus was observed in two of six cases. In the other four cases, a temporal increase of viral load was observed, but it rapidly fell below the detection limit. However, virus suppression was maintained in three cases following treatment termination, but with TNF-α stimulation, no rebound was seen only in one case (Figure 4F). Meanwhile, for patients, starting a treatment during the early stage of acute infection may be effective to reduce the reservoir size *in vivo*. In another experiment shown in Figures 4G and 4H, cells were initially treated with PEP005 and EFdA, then changed to EFdA only, and then treatment was discontinued for observation. In this experiment, no virus rebound was observed in four out of six cases when observation was terminated on week 26. Taken together, in this WIPE assay, the combined use of LRAs with ART drugs in the early stage of HIV-1 infection may be important to eliminate HIV latently infected cells. These *in vitro* data may suggest that, ideally, *in vivo* treatment aimed for HIV-1 cure should be initiated during the acute phase of the infection.

We observed the accumulation of defective proviruses or replication-incompetent proviruses within few months and found a cell clone with intact (without defection) proviruses that failed to produce HIV-1 mRNA in the model under treatment (Figures 7G and 7H). Kearney and co-workers demonstrated that only 7% of proviruses expressed HIV mRNA from HIV-infected donors (Wiegand et al., 2017). Also, Anderson et al. (2020) showed that the increase of gag-deleted proviruses occurred only after 1–2 years of therapy, and the number of defective proviruses increases after 10–15 years of therapy. Notably, EFdA (RT inhibitor) treatment may increase the number of defective proviruses. Indeed, as shown in Figure 7C, a nine-week treatment with EFdA alone targeted defective HIV-1 proviruses (20%); it is possible that RT inhibition resulted in the increased production of HIV-DNA with mutations including defection. In this regard, we found that the proviral DNAs from EFdA-treated samples (experiment 1, on week 17) contained an M184I mutation in the RT region (Figure S4E). M184V/I are known as resistant mutations against RT inhibitors and are also associated with resistance to EFdA (Maeda et al., 2014). The replication capacity of the EFdA-escape virus is diminished compared with the wild-type HIV-1 (Figure S4F). In addition, we examined drug sensitivity to EFdA of the EFdA-escape virus obtained from EFdA-treated cells and found a moderate decrease (~ten-fold) in the sensitivity to EFdA (Figure S4G). The result suggests that the inhibition of RT

(C and D) The expression of HIV-1 p24 and cell apoptosis during early phase of drug treatment. Bar graphs show the change in the percentage of cells expressing intracellular HIV-1 p24 (C) and annexin V (D) in the initial 24 h of drug treatment.

(E) Percentages of active caspase-3-positive cells in the p24-positive or p24-negative cell population.

(F) Percentages of full-length-type HIV-1 provirus after three weeks of drug treatment.

(G) Sorting of GFP-positive cells among HIV-1-infected Jurkat-LTR-GFP cells. GFP-positive (Tat^+) or GFP-negative populations (Tat^-) among HIV-1-infected Jurkat-LTR-GFP cells were sorted.

(H) GFP-negative cells were stimulated with 10 ng/mL TNF-α for 6 h and *gag* mRNA expression was quantified.

(I) GFP expression in sorted GFP-negative Jurkat-LTR-GFP cells infected with $HIV\text{-}1_{NL4\text{-}3}$ was analyzed after 6 h of TNF-α stimulation (10 ng/mL). Data represent the mean ± SD of three independent experiments.

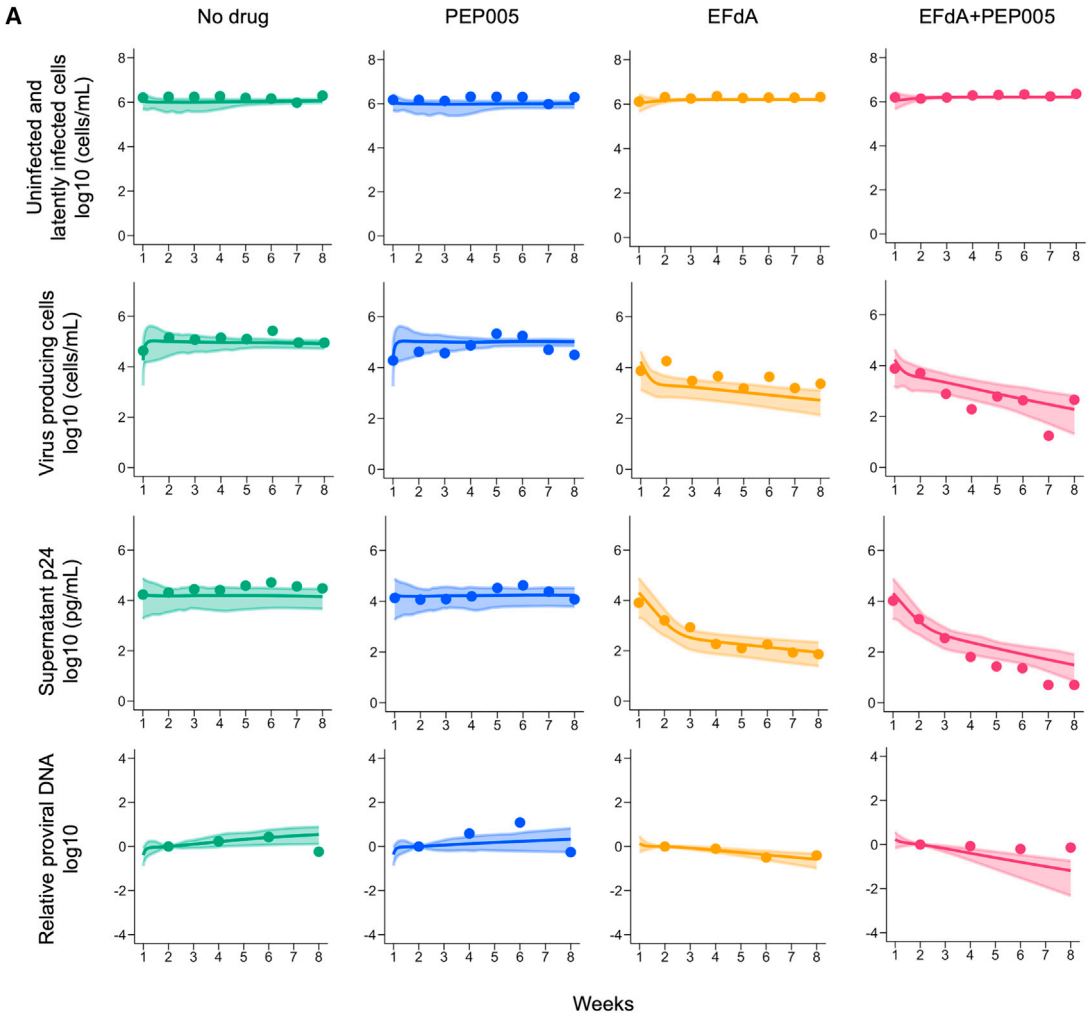

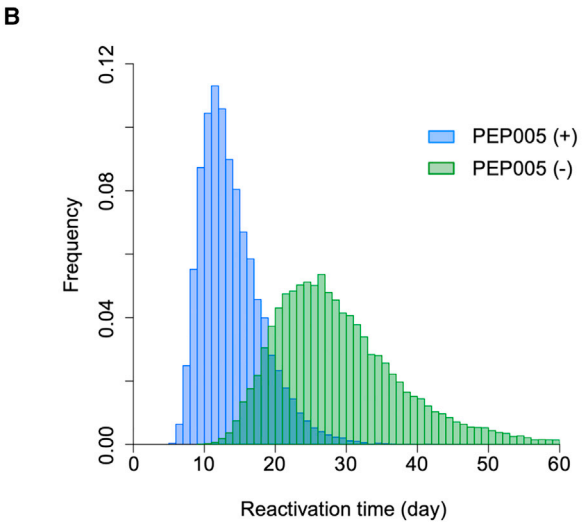

(legend on next page)

by a drug may increase the occurrence of mutations/defections in proviruses, which may help eliminate replication-competent proviruses. The LRA PEP005 is used, among other things, for precancerous actinic keratosis and is highly toxic when administered intravascularly. Therefore, LRAs with less side effects should be developed and used for future HIV-1 treatment.

We used the CXCR4-tropic (X4-tropic) HIV-1 variant NL4-3 to infect a T cell-derived Jurkat cell line. There is emerging evidence showing the importance of HIV-1-latency in monocytes or macrophages with the CCR5-tropic (R5-tropic) HIV-1 variant (Ganor et al., 2019). Thus, we obtained PM1CCR5 cells infected with R5-tropic HIV-1_{JRFL} (PM1CCR5/JRFL) but failed to maintain long-term chronic infection to evaluate drug efficacy (data not shown). For future studies, cell culture models with R5-tropic HIV-1-infected, monocyte-derived cells would be important for analyzing the differences in the latency mechanisms between the X4-tropic and R5-tropic HIV-1 variants.

In the WIPE assay, a $CD4^+$ T cell line of Jurkat cells was used as host cells; however, there is a wide variation in host $CD4^+$ T cells of infected individuals, which explains the different susceptibilities of HIV-1-infected $CD4^+$ T cell against various LRAs (Battivelli et al., 2018). Therefore, we propose the use of the WIPE assay to evaluate candidate LRA drugs for initial evaluation. Then, compounds with potent activity in the WIPE assay can be further evaluated by drug assays using primary $CD4^+$ T cell-derived HIV-1 latent reservoir models (Bosque and Planelles, 2009; Dobrowolski et al., 2019; Huang et al., 2018; Lassen et al., 2012; Saleh et al., 2007; Shan et al., 2012; Yang et al., 2009) or animal models (i.e., HIV-1-infected humanized mice or SIV-infected macaques) (Brooks et al., 2003; McBrien et al., 2020; Nixon et al., 2020). This strategy may increase the efficiency of LRA development and help to identify potent LRAs to reduce the reservoir size *in vivo*. Among various primary cell-derived latency models, Shan et al. (2012) reported a bcl-2-transduced HIV-1-infected $CD4^+$ T cell model, and using the model, they showed that the CTL-mediated elimination of HIV-1 reservoir cells was observed in the presence of autologous $CD8^+$ T cells. In this experiment, the elimination of HIV-1 reservoir cells only occurred with pre-stimulated $CD8^+$ T cells (but not with freshly isolated CTLs) to enhance CTL responses, suggesting that the CTL is another key factor for the shock and kill strategy (Huang et al., 2018; Shan et al., 2012). Dobrowolski et al. (2019) reported another HIV-1 latency model (the QUECEL model) that enabled us to obtain large numbers of HIV-1 latently infected $CD4^+$ T cells *in vitro*. A cocktail of cytokines, including TGF-β, IL-10, and IL-8, is used to generate the cell model with a homogeneous population of HIV-1 latently infected quiescent cells. However, on the other hand, these models require complicated steps to be established and cannot be used for long-term culture (more than four months) to determine the effect of drugs, including LRAs. Taken together, our findings provide a proof-of-concept for the shock and kill strategy against HIV-1 infection using our established *in vitro* assay. This cell culture system may have some advantages over other models, such as the HIV-1 latently infected cell lines (limited ISs, typically contain a reporter lacking important viral proteins), primary cell model (lower throughput), or animal models (resource demanding). A combination of persistent and heterogeneous HIV-1 infection in an *in vitro* model and high-throughput characterization of HIV-1 proviruses will help to develop a new generation of LRAs specific for HIV-1 proviral latency and for optimizing drug combinations to reduce the HIV-1 latently infected cells.

Limitations of the study

The study has some limitations. First, in this infection and treatment model, the elimination of HIV-1 latently infected cells occurs only through the apoptosis or CPE elicited by the reactivation, since no antiviral CTLs are involved in the model, which is clearly different from what is observed *in vivo.* In this study, we used an X4-tropic HIV-1 variant for the establishment of a chronically infected cell culture system (the WIPE assay). However, it is considered that the monocytes/macrophages infected with R5-tropic HIV-1 variants are also very important in forming reservoirs in the body. Thus, further analyses using cells infected with R5-tropic HIV-1s are needed. Although the WIPE assay successfully provided insights into the underlying mechanisms of HIV-1 latency, it is possible that the silencing mechanisms selected in immortalized cell lines differ from those selected in primary cells *in vivo*. Therefore, results from experiments using *in vivo* models also should be taken into account for the detailed analysis of the mechanisms of HIV-1 latency.

STAR★METHODS

Detailed methods are provided in the online version of this paper and include the following:

- KEY RESOURCES TABLE
- RESOURCE AVAILABILITY
  - Lead contact
  - Materials availability
  - Data and code availability
- EXPERIMENTAL MODEL AND SUBJECT DETAILS
  - Ethics statement
  - Cell culture
  - Drugs and reagents
- METHOD DETAILS
  - Establishment of the HIV-1 chronically infected cell culture model

Figure 6. HIV-1 infection dynamics with antiviral drugs in the WIPE assay

(A) Fitting of the mathematical model to the experimental data in the WIPE assay without and with antiviral drug(s): numbers of uninfected and latently infected cells (cells/mL), virus-producing cells (cells/mL), supernatant p24 (pg/mL), and normalized proviral DNA. The shadowed regions correspond to 95% posterior predictive intervals, the solid lines gave the best-fit solution (mean) for the mathematical model, and the colored dots show the experimental datasets. All data were fitted simultaneously.

(B) The distribution for the time until reactivation without and with PEP005 treatment calculated from all accepted MCMC parameter estimates is shown in green and blue, respectively. These lengths were significantly shorter with PEP005 treatment than without treatment, as assessed by the repeated bootstrap t test.

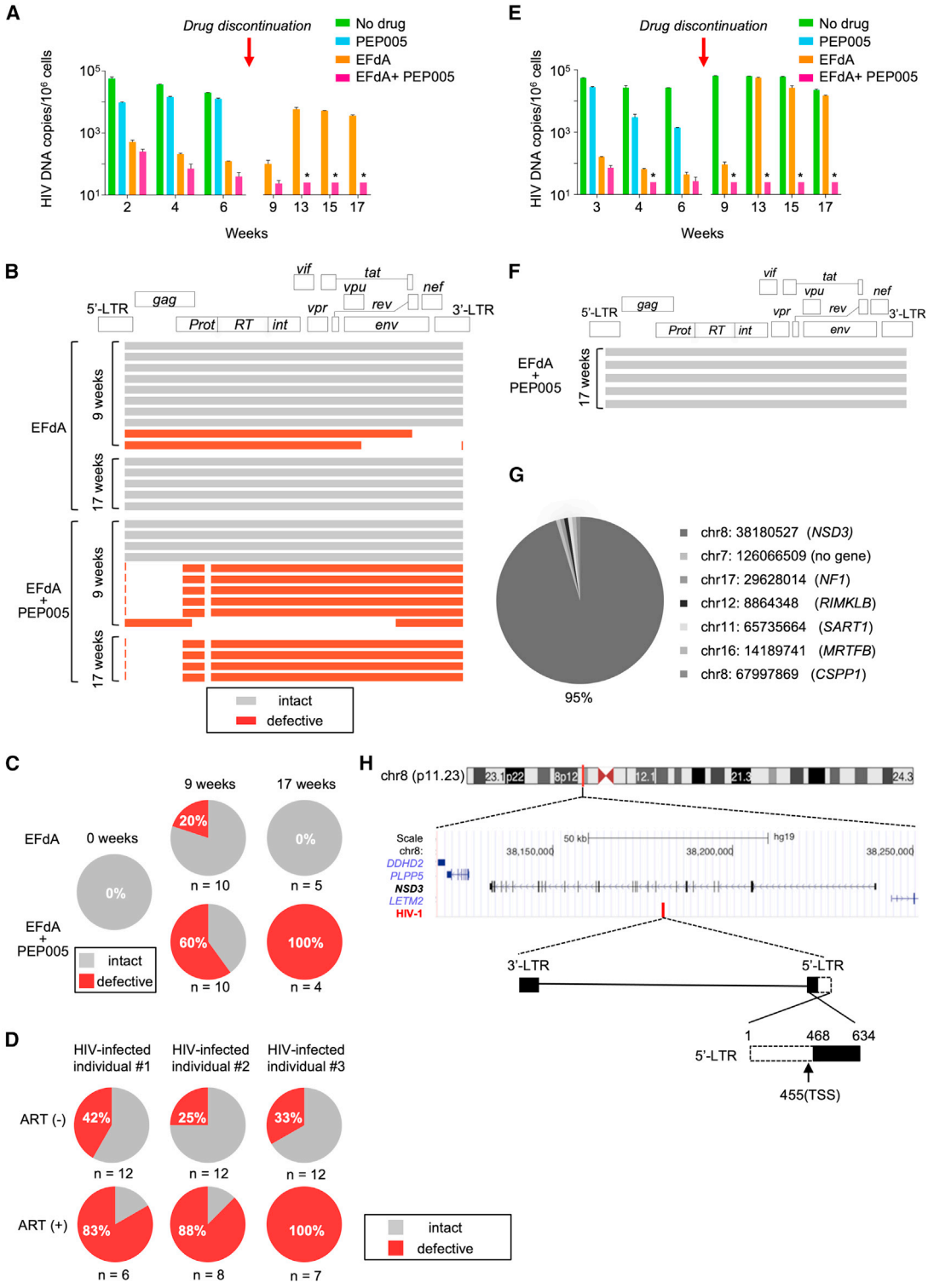

Figure 7. Mechanisms for the elimination of HIV-1 producible cells *in vitro*

(A) Quantification of intracellular copies of HIV-1 DNA at each time point in experiment 6 (Figure S2A).

(B) Schematic representation of the individual provirus structures from two different treatment groups and at two time points in experiment 6. Each horizontal bar represents an individual HIV-1 genome, as determined by amplification of near full-length HIV-1 DNA from a single HIV-1 genome and DNA sequencing. The gray bars denote full-length types, and the red bars indicate defective proviruses.

(C) Pie charts reflecting the proportion of defective and intact proviruses in experiment 6.

(legend continued on next page)

- HIV-1 reversal in latently infected cells and caspase-3 activation by LRAs
- Determination of antiviral activity of LRAs and conventional anti-HIV-1 drugs in Jurkat/NL cells (WIPE assay)
- Flow cytometry analysis
- HIV-flow
- Sorting of GFP^+ or GFP^- cells from HIV-1_{NL4-3}-infected JLTRG cells
- Isolation of PBMCs from HIV-1 infected individuals
- RT-qPCR for HIV-1 mRNA quantification
- Amplification of near-full-length single HIV-1 genome and sequencing
- Ligation-mediated PCR (LM-PCR)
- PCR-based HIV-1 RT enzyme assay
- Viral replication kinetics and drug susceptibility assay
- Bioinformatic analysis
- Mathematical modeling

● QUANTIFICATION AND STATISTICAL ANALYSIS

SUPPLEMENTAL INFORMATION

Supplemental information can be found online at https://doi.org/10.1016/j.crmeth.2021.100122.

ACKNOWLEDGMENTS

We thank Jumpei Ito for providing access to the Python program, allowing us to perform association analyses between the epigenetic environment and viral integration sites. We also thank Shinichi Oka for his advice and suggestions for the manuscript. We thank Editage (www.editage.jp) for English language editing. This research was supported in part by grants from the Japan Agency for Medical Research and Development (AMED) (grant nos. JP20fk0410015 to K.T., Y.S., and K. Maeda; JP19fk0410009 to Y.S.; JP21fk0410023 to K.T. and Y.S.; and JP19fk0410014 to Y.S.). Y.S. was also supported by grants from MEXT/JSPS KAKENHI (JP17890606). S. Iwami and Y.S. were supported by JST MIRAI. S. Iwami was also supported by Moonshot R&D (JPMJMS2021 and JPMJMS2025). K.T. and K. Maeda were also supported by a grant from the National Center for Global Health and Medicine, Japan (20A1018). K. Matsuda was supported by JSPS KAKENHI (grant no. 20K17480).

AUTHOR CONTRIBUTIONS

K.Y., Y.S., and K. Maeda designed the study. K. Matsuda, S. Islam, K.T., S.H., H.K., M.M., K.S., and N.S.D. performed the experiments. S.M. provided clinical sample DNA. S. Islam, B.J.Y.T., and Y.S. performed bioinformatic analysis. T.T., K.K., K.S.K., and S. Iwami performed mathematical analysis. H.G., K.Y., S.M., H.M., Y.S., and K. Maeda supervised the work. Y.S. and K. Maeda wrote the manuscript with input from all authors.

DECLARATION OF INTERESTS

Shingo Iwami is an employee of Science Groove Inc. The other authors declare that the research was conducted in the absence of any commercial or financial relationship that could be construed as a potential conflict of interest.

Received: May 31, 2021
Revised: August 18, 2021
Accepted: November 5, 2021
Published: November 29, 2021

SUPPORTING CITATIONS

The following references appear in the supplemental information: Douek et al., 2002; Goff et al., 2000.

REFERENCES

Anderson, E.M., Simonetti, F.R., Gorelick, R.J., Hill, S., Gouzoulis, M.A., Bell, J., Rehm, C., Perez, L., Boritz, E., Wu, X., et al. (2020). Dynamic shifts in the HIV proviral landscape during long term combination antiretroviral therapy: implications for persistence and control of HIV infections. Viruses *12*, 136.

Archin, N.M., Liberty, A.L., Kashuba, A.D., Choudhary, S.K., Kuruc, J.D., Crooks, A.M., Parker, D.C., Anderson, E.M., Kearney, M.F., Strain, M.C., et al. (2012). Administration of vorinostat disrupts HIV-1 latency in patients on antiretroviral therapy. Nature *487*, 482–485.

Badley, A.D., Sainski, A., Wightman, F., and Lewin, S.R. (2013). Altering cell death pathways as an approach to cure HIV infection. Cell Death Dis. *4*, e718.

Battivelli, E., Dahabieh, M.S., Abdel-Mohsen, M., Svensson, J.P., Tojal Da Silva, I., Cohn, L.B., Gramatica, A., Deeks, S., Greene, W.C., Pillai, S.K., et al. (2018). Distinct chromatin functional states correlate with HIV latency reactivation in infected primary CD4(+) T cells. eLife *7*, e34655.

Borducchi, E.N., Liu, J., Nkolola, J.P., Cadena, A.M., Yu, W.H., Fischinger, S., Broge, T., Abbink, P., Mercado, N.B., Chandrashekar, A., et al. (2018). Antibody and TLR7 agonist delay viral rebound in SHIV-infected monkeys. Nature *563*, 360–364.

Bosque, A., and Planelles, V. (2009). Induction of HIV-1 latency and reactivation in primary memory CD4+ T cells. Blood *113*, 58–65.

Brooks, D.G., Hamer, D.H., Arlen, P.A., Gao, L., Bristol, G., Kitchen, C.M., Berger, E.A., and Zack, J.A. (2003). Molecular characterization, reactivation, and depletion of latent HIV. Immunity *19*, 413–423.

Bruner, K.M., Murray, A.J., Pollack, R.A., Soliman, M.G., Laskey, S.B., Capoferri, A.A., Lai, J., Strain, M.C., Lada, S.M., Hoh, R., et al. (2016). Defective proviruses rapidly accumulate during acute HIV-1 infection. Nat. Med. *22*, 1043–1049.

Bullen, C.K., Laird, G.M., Durand, C.M., Siliciano, J.D., and Siliciano, R.F. (2014). New ex vivo approaches distinguish effective and ineffective single agents for reversing HIV-1 latency in vivo. Nat. Med. *20*, 425–429.

Butler, S.L., Hansen, M.S., and Bushman, F.D. (2001). A quantitative assay for HIV DNA integration in vivo. Nat. Med. *7*, 631–634.

Chun, T.W., Stuyver, L., Mizell, S.B., Ehler, L.A., Mican, J.A., Baseler, M., Lloyd, A.L., Nowak, M.A., and Fauci, A.S. (1997). Presence of an inducible HIV-1 latent reservoir during highly active antiretroviral therapy. Proc. Natl. Acad. Sci. U S A *94*, 13193–13197.

Cohn, L.B., Silva, I.T., Oliveira, T.Y., Rosales, R.A., Parrish, E.H., Learn, G.H., Hahn, B.H., Czartoski, J.L., McElrath, M.J., Lehmann, C., et al. (2015). HIV-1 integration landscape during latent and active infection. Cell *160*, 420–432.

Darcis, G., Van Driessche, B., and Van Lint, C. (2017). HIV latency: should we shock or lock? Trends Immunol. *38*, 217–228.

Deeks, S.G. (2012). HIV: shock and kill. Nature *487*, 439–440.

(D) Pie charts reflecting the proportion of defective and intact proviruses in PBMCs from three HIV-1-infected individuals.
(E) Quantification of intracellular copies of HIV-1 DNA at each time point in experiment 1 (Figure 3D).
(F) Schematic representation of the individual provirus structures in experiment 1 for the EFdA/PEP005 culture group 17 weeks after drug treatment initiation.
(G) Pie chart showing the relative abundance of each HIV-1-infected clone. Chromosomal number and position of each clone are shown in the right panel.
(H) Schematic figure of the provirus structure and IS in the expanded clone. A 467-basepair deletion in the 5′ end of 5′ LTR was observed. TSS, transcription start site. Asterisk (*) represents below detection limit.

Dobrowolski, C., Valadkhan, S., Graham, A.C., Shukla, M., Ciuffi, A., Telenti, A., and Karn, J. (2019). Entry of polarized effector cells into quiescence forces HIV latency. mBio *10*, e00337-19.

Douek, D.C., Brenchley, J.M., Betts, M.R., Ambrozak, D.R., Hill, B.J., Okamoto, Y., Casazza, J.P., Kuruppu, J., Kunstman, K., Wolinsky, S., et al. (2002). HIV preferentially infects HIV-specific CD4+ T cells. Nature *417*, 95–98.

Edgar, R.C. (2004). MUSCLE: multiple sequence alignment with high accuracy and high throughput. Nucleic Acids Res. *32*, 1792–1797.

Efron, B., and Tibshirani, R.J. (1994). An Introduction to the Bootstrap (CRC Press).

Einkauf, K.B., Lee, G.Q., Gao, C., Sharaf, R., Sun, X., Hua, S., Chen, S.M., Jiang, C., Lian, X., Chowdhury, F.Z., et al. (2019). Intact HIV-1 proviruses accumulate at distinct chromosomal positions during prolonged antiretroviral therapy. J. Clin. Invest. *129*, 988–998.

Finzi, D., Hermankova, M., Pierson, T., Carruth, L.M., Buck, C., Chaisson, R.E., Quinn, T.C., Chadwick, K., Margolick, J., Brookmeyer, R., et al. (1997). Identification of a reservoir for HIV-1 in patients on highly active antiretroviral therapy. Science *278*, 1295–1300.

Ganor, Y., Real, F., Sennepin, A., Dutertre, C.A., Prevedel, L., Xu, L., Tudor, D., Charmeteau, B., Couedel-Courteille, A., Marion, S., et al. (2019). HIV-1 reservoirs in urethral macrophages of patients under suppressive antiretroviral therapy. Nat. Microbiol. *4*, 633–644.

Gillet, N.A., Malani, N., Melamed, A., Gormley, N., Carter, R., Bentley, D., Berry, C., Bushman, F.D., Taylor, G.P., and Bangham, C.R. (2011). The host genomic environment of the provirus determines the abundance of HTLV-1-infected T-cell clones. Blood *117*, 3113–3122.

Goff, L.K., Neat, M.J., Crawley, C.R., Jones, L., Jones, E., Lister, T.A., and Gupta, R.K. (2000). The use of real-time quantitative polymerase chain reaction and comparative genomic hybridization to identify amplification of the REL gene in follicular lymphoma. Br. J. Haematol. *111*, 618–625.

Haario, H., Laine, M., Mira, A., and Saksman, E. (2006). DRAM: efficient adaptive MCMC. Stat. Comput. *16*, 339–354.

Han, Y., Lassen, K., Monie, D., Sedaghat, A.R., Shimoji, S., Liu, X., Pierson, T.C., Margolick, J.B., Siliciano, R.F., and Siliciano, J.D. (2004). Resting CD4+ T cells from human immunodeficiency virus type 1 (HIV-1)-infected individuals carry integrated HIV-1 genomes within actively transcribed host genes. J. Virol. *78*, 6122–6133.

Han, Y., Lin, Y.B., An, W., Xu, J., Yang, H.C., O'Connell, K., Dordai, D., Boeke, J.D., Siliciano, J.D., and Siliciano, R.F. (2008). Orientation-dependent regulation of integrated HIV-1 expression by host gene transcriptional readthrough. Cell Host Microbe *4*, 134–146.

Hattori, S.I., Matsuda, K., Tsuchiya, K., Gatanaga, H., Oka, S., Yoshimura, K., Mitsuya, H., and Maeda, K. (2018). Combination of a latency-reversing agent with a Smac mimetic minimizes secondary HIV-1 infection in vitro. Front. Microbiol. *9*, 2022.

Ho, Y.C., Shan, L., Hosmane, N.N., Wang, J., Laskey, S.B., Rosenbloom, D.I., Lai, J., Blankson, J.N., Siliciano, J.D., and Siliciano, R.F. (2013). Replication-competent noninduced proviruses in the latent reservoir increase barrier to HIV-1 cure. Cell *155*, 540–551.

Hu, Y., Yan, C., Hsu, C.H., Chen, Q.R., Niu, K., Komatsoulis, G.A., and Meerzaman, D. (2014). OmicCircos: a simple-to-use R package for the circular visualization of multidimensional omics data. Cancer Inform. *13*, 13–20.

Huang, S.H., Ren, Y., Thomas, A.S., Chan, D., Mueller, S., Ward, A.R., Patel, S., Bollard, C.M., Cruz, C.R., Karandish, S., et al. (2018). Latent HIV reservoirs exhibit inherent resistance to elimination by CD8+ T cells. J. Clin. Invest. *128*, 876–889.

Imamichi, H., Dewar, R.L., Adelsberger, J.W., Rehm, C.A., O'Doherty, U., Paxinos, E.E., Fauci, A.S., and Lane, H.C. (2016). Defective HIV-1 proviruses produce novel protein-coding RNA species in HIV-infected patients on combination antiretroviral therapy. Proc. Natl. Acad. Sci. U S A *113*, 8783–8788.

Imamichi, H., Smith, M., Adelsberger, J.W., Izumi, T., Scrimieri, F., Sherman, B.T., Rehm, C.A., Imamichi, T., Pau, A., Catalfamo, M., et al. (2020). Defective HIV-1 proviruses produce viral proteins. Proc. Natl. Acad. Sci. U S A *117*, 3704–3710.

Iwami, S., Holder, B.P., Beauchemin, C.A., Morita, S., Tada, T., Sato, K., Igarashi, T., and Miura, T. (2012). Quantification system for the viral dynamics of a highly pathogenic simian/human immunodeficiency virus based on an in vitro experiment and a mathematical model. Retrovirology *9*, 18.

Iwami, S., Takeuchi, J.S., Nakaoka, S., Mammano, F., Clavel, F., Inaba, H., Kobayashi, T., Misawa, N., Aihara, K., Koyanagi, Y., et al. (2015). Cell-to-cell infection by HIV contributes over half of virus infection. eLife *4*, e08150.

Katsuya, H., Cook, L.B.M., Rowan, A.G., Melamed, A., Turpin, J., Ito, J., Islam, S., Miyazato, P., Jek Yang Tan, B., Matsuo, M., Miyakawa, T., Nakata, H., Matsushita, S., Taylor, G.P., Bangham, C.R.M., Kimura, S., and Satou, Y. (2021). Clonality of HIV-1 and HTLV-1 infected cells in naturally coinfected individuals. J. Infect Dis. https://doi.org/10.1093/infdis/jiab202.

Kessing, C.F., Nixon, C.C., Li, C., Tsai, P., Takata, H., Mousseau, G., Ho, P.T., Honeycutt, J.B., Fallahi, M., Trautmann, L., et al. (2017). In vivo suppression of HIV rebound by didehydro-cortistatin A, a "block-and-lock" strategy for HIV-1 treatment. Cell Rep. *21*, 600–611.

Kim, Y., Anderson, J.L., and Lewin, S.R. (2018). Getting the "kill" into "shock and kill": strategies to eliminate latent HIV. Cell Host Microbe *23*, 14–26.

Laird, G.M., Bullen, C.K., Rosenbloom, D.I., Martin, A.R., Hill, A.L., Durand, C.M., Siliciano, J.D., and Siliciano, R.F. (2015). Ex vivo analysis identifies effective HIV-1 latency-reversing drug combinations. J. Clin. Invest. *125*, 1901–1912.

Lassen, K.G., Hebbeler, A.M., Bhattacharyya, D., Lobritz, M.A., and Greene, W.C. (2012). A flexible model of HIV-1 latency permitting evaluation of many primary CD4 T-cell reservoirs. PLoS One *7*, e30176.

Lee, G.Q., Orlova-Fink, N., Einkauf, K., Chowdhury, F.Z., Sun, X., Harrington, S., Kuo, H.H., Hua, S., Chen, H.R., Ouyang, Z., et al. (2017). Clonal expansion of genome-intact HIV-1 in functionally polarized Th1 CD4+ T cells. J. Clin. Invest. *127*, 2689–2696.

Lenasi, T., Contreras, X., and Peterlin, B.M. (2008). Transcriptional interference antagonizes proviral gene expression to promote HIV latency. Cell Host Microbe *4*, 123–133.

Li, H., and Durbin, R. (2009). Fast and accurate short read alignment with Burrows-Wheeler transform. Bioinformatics *25*, 1754–1760.

Liu, R., Yeh, Y.J., Varabyou, A., Collora, J.A., Sherrill-Mix, S., Talbot, C.C., Jr., Mehta, S., Albrecht, K., Hao, H., Zhang, H., et al. (2020). Single-cell transcriptional landscapes reveal HIV-1-driven aberrant host gene transcription as a potential therapeutic target. Sci. Transl. Med. *12*, eaaz0802.

Maeda, K., Desai, D.V., Aoki, M., Nakata, H., Kodama, E.N., and Mitsuya, H. (2014). Delayed emergence of HIV-1 variants resistant to 4'-ethynyl-2-fluoro-2'-deoxyadenosine: comparative sequential passage study with lamivudine, tenofovir, emtricitabine and BMS-986001. Antivir. Ther. *19*, 179–189.

Maldarelli, F., Wu, X., Su, L., Simonetti, F.R., Shao, W., Hill, S., Spindler, J., Ferris, A.L., Mellors, J.W., Kearney, M.F., et al. (2014). HIV latency. Specific HIV integration sites are linked to clonal expansion and persistence of infected cells. Science *345*, 179–183.

Matsuda, K., Kobayakawa, T., Tsuchiya, K., Hattori, S.I., Nomura, W., Gatanaga, H., Yoshimura, K., Oka, S., Endo, Y., Tamamura, H., et al. (2019). Benzolactam-related compounds promote apoptosis of HIV-infected human cells via protein kinase C-induced HIV latency reversal. J. Biol. Chem. *294*, 116–129.

McBrien, J.B., Mavigner, M., Franchitti, L., Smith, S.A., White, E., Tharp, G.K., Walum, H., Busman-Sahay, K., Aguilera-Sandoval, C.R., Thayer, W.O., et al. (2020). Robust and persistent reactivation of SIV and HIV by N-803 and depletion of CD8(+) cells. Nature *578*, 154–159.

Nakata, H., Amano, M., Koh, Y., Kodama, E., Yang, G., Bailey, C.M., Kohgo, S., Hayakawa, H., Matsuoka, M., Anderson, K.S., et al. (2007). Activity against human immunodeficiency virus type 1, intracellular metabolism, and effects on human DNA polymerases of 4'-ethynyl-2-fluoro-2'-deoxyadenosine. Antimicrob. Agents Chemother. *51*, 2701–2708.

Nixon, C.C., Mavigner, M., Sampey, G.C., Brooks, A.D., Spagnuolo, R.A., Irlbeck, D.M., Mattingly, C., Ho, P.T., Schoof, N., Cammon, C.G., et al. (2020). Systemic HIV and SIV latency reversal via non-canonical NF-kappaB signalling in vivo. Nature *578*, 160–165.

Pardons, M., Baxter, A.E., Massanella, M., Pagliuzza, A., Fromentin, R., Dufour, C., Leyre, L., Routy, J.P., Kaufmann, D.E., and Chomont, N. (2019). Single-cell characterization and quantification of translation-competent viral reservoirs in treated and untreated HIV infection. Plos Pathog. *15*, e1007619.

Perelson, A.S. (2002). Modelling viral and immune system dynamics. Nat. Rev. Immunol. *2*, 28–36.

Perelson, A.S., Essunger, P., Cao, Y., Vesanen, M., Hurley, A., Saksela, K., Markowitz, M., and Ho, D.D. (1997). Decay characteristics of HIV-1-infected compartments during combination therapy. Nature *387*, 188–191.

Plummer, M., Best, N., Cowles, K., and Vines, K. (2006). CODA: convergence diagnosis and output analysis for MCMC. R. News *6*, 7–11.

R Core Team (2019). R: A Language and Environment for Statistical Computing (R Foundation for Statistical Computing).

Robinson, J.T., Thorvaldsdottir, H., Winckler, W., Guttman, M., Lander, E.S., Getz, G., and Mesirov, J.P. (2011). Integrative genomics viewer. Nat. Biotechnol. *29*, 24–26.

Rong, L., and Perelson, A.S. (2009). Modeling latently infected cell activation: viral and latent reservoir persistence, and viral blips in HIV-infected patients on potent therapy. Plos Comput. Biol. *5*, e1000533.

Saleh, S., Solomon, A., Wightman, F., Xhilaga, M., Cameron, P.U., and Lewin, S.R. (2007). CCR7 ligands CCL19 and CCL21 increase permissiveness of resting memory CD4+ T cells to HIV-1 infection: a novel model of HIV-1 latency. Blood *110*, 4161–4164.

Sanchez, G., Xu, X., Chermann, J.C., and Hirsch, I. (1997). Accumulation of defective viral genomes in peripheral blood mononuclear cells of human immunodeficiency virus type 1-infected individuals. J. Virol. *71*, 2233–2240.

Satou, Y., Katsuya, H., Fukuda, A., Misawa, N., Ito, J., Uchiyama, Y., Miyazato, P., Islam, S., Fassati, A., Melamed, A., et al. (2017). Dynamics and mechanisms of clonal expansion of HIV-1-infected cells in a humanized mouse model. Sci. Rep. *7*, 6913.

Schroder, A.R., Shinn, P., Chen, H., Berry, C., Ecker, J.R., and Bushman, F. (2002). HIV-1 integration in the human genome favors active genes and local hotspots. Cell *110*, 521–529.

Shan, L., Deng, K., Shroff, N.S., Durand, C.M., Rabi, S.A., Yang, H.C., Zhang, H., Margolick, J.B., Blankson, J.N., and Siliciano, R.F. (2012). Stimulation of HIV-1-specific cytolytic T lymphocytes facilitates elimination of latent viral reservoir after virus reactivation. Immunity *36*, 491–501.

Soetaert, K., and Petzoldt, T. (2010). Inverse modelling, sensitivity and Monte Carlo analysis in R using package FME. J. Stat. Softw. *33*, 1–28.

Spina, C.A., Anderson, J., Archin, N.M., Bosque, A., Chan, J., Famiglietti, M., Greene, W.C., Kashuba, A., Lewin, S.R., Margolis, D.M., et al. (2013). An in-depth comparison of latent HIV-1 reactivation in multiple cell model systems and resting CD4+ T cells from aviremic patients. PLoS Pathog. *9*, e1003834.

Spivak, A.M., Andrade, A., Eisele, E., Hoh, R., Bacchetti, P., Bumpus, N.N., Emad, F., Buckheit, R., 3rd, McCance-Katz, E.F., Lai, J., et al. (2014). A pilot study assessing the safety and latency-reversing activity of disulfiram in HIV-1-infected adults on antiretroviral therapy. Clin. Infect. Dis. *58*, 883–890.

Tyagi, M., Pearson, R.J., and Karn, J. (2010). Establishment of HIV latency in primary CD4+ cells is due to epigenetic transcriptional silencing and P-TEFb restriction. J. Virol. *84*, 6425–6437.

Vibholm, L.K., Konrad, C.V., Schleimann, M.H., Frattari, G., Winckelmann, A., Klastrup, V., Jensen, N.M., Jensen, S.S., Schmidt, M., Wittig, B., et al. (2019). Effects of 24-week Toll-like receptor 9 agonist treatment in HIV type 1+ individuals. AIDS *33*, 1315–1325.

Wagner, T.A., McLaughlin, S., Garg, K., Cheung, C.Y., Larsen, B.B., Styrchak, S., Huang, H.C., Edlefsen, P.T., Mullins, J.I., and Frenkel, L.M. (2014). HIV latency. Proliferation of cells with HIV integrated into cancer genes contributes to persistent infection. Science *345*, 570–573.

Wiegand, A., Spindler, J., Hong, F.F., Shao, W., Cyktor, J.C., Cillo, A.R., Halvas, E.K., Coffin, J.M., Mellors, J.W., and Kearney, M.F. (2017). Single-cell analysis of HIV-1 transcriptional activity reveals expression of proviruses in expanded clones during ART. Proc. Natl. Acad. Sci. U S A *114*, E3659–E3668.

Wong, J.K., Hezareh, M., Gunthard, H.F., Havlir, D.V., Ignacio, C.C., Spina, C.A., and Richman, D.D. (1997). Recovery of replication-competent HIV despite prolonged suppression of plasma viremia. Science *278*, 1291–1295.

Yang, H.C., Xing, S., Shan, L., O'Connell, K., Dinoso, J., Shen, A., Zhou, Y., Shrum, C.K., Han, Y., Liu, J.O., et al. (2009). Small-molecule screening using a human primary cell model of HIV latency identifies compounds that reverse latency without cellular activation. J. Clin. Invest. *119*, 3473–3486.

Yasutake, Y., Hattori, S.I., Hayashi, H., Matsuda, K., Tamura, N., Kohgo, S., Maeda, K., and Mitsuya, H. (2018). HIV-1 with HBV-associated Q151M substitution in RT becomes highly susceptible to entecavir: structural insights into HBV-RT inhibition by entecavir. Sci. Rep. *8*, 1624.

STAR★METHODS

KEY RESOURCES TABLE

REAGENT or RESOURCE	SOURCE	IDENTIFIER
Antibodies		
Anti-HIV-1 p24-FITC mAb (24-4)	Santa Cruz Biotechnology	Cat# sc-69728 FITC; RRID: AB_1125169
Anti-HIV-1 p24-PE mAb (KC57)	Beckman Coulter	Cat# 6604667; RRID: AB_1575989
Anti-HIV-1 p24-APC mAb (28B7)	MediMabs	Cat# MM-0289-APC
Alexafluor 647-conjugated anti-active caspase-3 mAb (C92-605)	BD Pharmingen	Cat# 560626; RRID: AB_1727414
Bacterial and virus strains		
HIV-1 NL4-3 Infectious Molecular Clone (pNL-43)	NIH AIDS Reagent Program	Cat# ARP-114
HIV-1 JR-FL Infectious Molecular Clone (pJR-FL)	Kindly provided by Dr. Yoshio Koyanagi	N/A
Biological samples		
Human PBMCs from HIV-1 infected individuals	National Center for Global Health and Medicine Hospital	N/A
Human PBMCs from HIV-1 infected individuals	Kumamoto University Hospital	N/A
Chemicals, peptides, and recombinant proteins		
RPMI 1640	Sigma-Aldrich	Cat# R8758
Fetal calf serum (FCS)	Sigma-Aldrich	Cat# 172012
Phosphate buffered salts (PBS)	Wako Pure Chemical	Cat# 045-29795
Ficoll-Paque PLUS	GE Healthcare	Cat# 17-1440-02
4% Paraformaldehyde Phosphate Buffer Solution	Wako Pure Chemical	Cat# 163-20145
Flow cytometry perm buffer	TONBO Biosciences	Cat# TNB-1213-L150
Ghost Dye Violet 450	TONBO Biosciences	Cat# 13-0863
Ghost Dye Red 780	TONBO Biosciences	Cat# 13-0865
PI solution	BioLegend	Cat# 421301
FITC annexin V	BioLegend	Cat# 640906
Annexin V binding buffer	BioLegend	Cat# 422201
EFdA/MK-8591/ISL	Nakata et al. (2007)	N/A
DRV	Selleck	Cat# S5250
DTG	Selleck	Cat# S2667
PEP005	Cayman Chemical	Cat# 16207
SAHA/Vorinostat	Santa Cruz Biotechnology	Cat# sc-220139
JQ-1	BioVision	Cat# 2070
GSK525762A	ChemScene	Cat# CS-0028499
Ro5-3335	Merck	Cat# 219506
Prostratin	Sigma-Aldrich	Cat# P0077
Bryostatin-1	Sigma-Aldrich	Cat# B7431
AI-10-49	MedChem Express	Cat# HY-16786
Panobinostat	MedChem Express	Cat# HY-10224
GS-9620	MedChem Express	Cat# HY-15601
Birinapant	MedChem Express	Cat# HY-16591
Phorbole 12-myristate13-acetate/PMA	Wako Pure Chemical	Cat# 162-23591
Recombinant Human TNF-α	BioLegend	Cat# 570106
AMPure XP	Beckman Coulter	Cat# A63880
Tris-HCl (pH 7.4)	Wako Pure Chemical	Cat# MB-002
$MgCl_2$	Nacalai Tesque	Cat# 20908-65

(*Continued on next page*)

Continued

REAGENT or RESOURCE	SOURCE	IDENTIFIER
DTT	Wako Pure Chemical	Cat# 040-29223
Triton X-100	Nacalai Tesque	Cat# 35501-02
MuLV RT buffer	New England Biolabs	Cat# B0253S
dNTPs	TaKaRa Bio	Cat# 4030
Recombinant RNase inhibitor	TaKaRa Bio	Cat# 2313A
MS2 RNA	Roche	Cat# 10165948001
Recombinant HIV-1 RT	Bio Academia	Cat# 05-001
Critical commercial assays		
Lumipulse HIV Ag/Ab kit	FUJIREBIO	Cat# 295335
Roche COBAS AmpliPrep/COBAS TaqMan HIV-1 Test version 2.0	Roche	Cat# 518-495862
QIAmp DNA Blood mini kit	Qiagen	Cat# 51104
RNeasy Mini Kit	Qiagen	Cat# 74004
Premix Ex Taq (Probe qPCR) ROX plus	Takara Bio	Cat# RR39LR
PrimeScript RT Master Mix	Takara Bio	Cat# RR036A
Takara Ex Taq hot start version	Takara Bio	Cat# R007A
PowerUp SYBR Green Master Mix	Applied Biosystems	Cat# A25742
QIAquick PCR Purification Kit	Qiagen	Cat# 28104
NEBNext Ultra II DNA Library Prep Kit for Illumina	New England Biolabs	Cat# E7645S
Qubit dsDNA High Sensitivity Assay kit	Invitrogen	Cat# Q32851
Library quality check by TapeStation	Agilent Technologies	https://www.agilent.com/en/promotions/agilent-2200-tapestation-system
GenNext NGS Library Quantification kit	TOYOBO	Cat# NLQ-101
MinION platform with Flow Cell R9.4.1	Oxford Nanopore Technologies	Cat# FLO-MIN106D
Rapid Barcoding kit	Oxford Nanopore Technologies	Cat# SQK-RBK004
NEBNext Ultra II End Repair/dA-Tailing Module	New England Biolabs	Cat# E7546S
Cell Counting Kit-8	Dojindo	Cat# CK04
Deposited data		
Fastq of all samples	This study	DRA accession number: DRA012587 DRA012818
Experimental models: Cell lines		
Human: Jurkat cells	ATCC	Cat# TIB-152
Human: Jurkat-LTR-GFP cells	NIH AIDS Reagent Program	Cat# ARP-11587
Human: MT-4 cells	NIH AIDS Reagent Program	Cat# ARP-120
Human: Hut78 cells	ATCC	Cat# TIB-161
Human: MOLT4 cells	ATCC	Cat# CRL-1582
Human: PM1-CCR5 cells	Kindly provided by Dr. Yosuke Maeda	N/A
Software and algorithms		
FlowJo	Tree Star	https://www.flowjo.com
Prism 8	GraphPad Software	https://www.graphpad.com/
BWA-MEM algorithm	Li and Durbin (2009)	http://bio-bwa.sourceforge.net/
Samtools	Li and Durbin (2009)	http://samtools.sourceforge.net/
Picard	Broad Institute of MIT and Harvard	http://broadinstitute.github.io/picard/
Integrative Genomics Viewer	Robinson et al. (2011)	http://software.broadinstitute.org/software/igv/
EPI2ME software	Oxford Nanopore Technologies	https://epi2me.nanoporetech.com/
R Statistical Computing software	The R Foundation	https://www.r-project.org

RESOURCE AVAILABILITY

Lead contact

Further information and requests for resources and reagents should be directed to and will be fulfilled by the lead contact, Kenji Maeda (kmaeda@ri.ncgm.go.jp).

Materials availability

All unique reagents generated in this study are listed in the key resources table and available from the lead contact with a completed Materials Transfer Agreement.

Data and code availability

- All sequencing data sets generated by this study were deposited in the DDBJ sequence Read Archive (accession number: DRA012587, DRA012818). These are also noted in key resources table.
- Integration site analysis is performed as previously reported (Katsuya et al., 2021), and the codes are available for download from https://github.com/satoulab/coinfection_J.Infect.Dis.
- Any additional information required to reanalyze the data reported in this paper is available from the lead contact upon request.

EXPERIMENTAL MODEL AND SUBJECT DETAILS

Ethics statement

The study was performed in accordance with the guidelines of the Declaration of Helsinki. Analysis of the clinical sample shown in Figure 1F was conducted based on a protocol reviewed and approved by the Kumamoto University (Kumamoto, Japan) Institutional Review Board (approval number Genome 258).

Peripheral blood samples analyzed as shown in Figure S3 were collected from individuals infected with HIV-1 before or after receiving cART for at least 7 years. The Ethics Committee of the National Center for Global Health and Medicine (Tokyo, Japan) approved this study (NCGM-G-002259-00).

Cell culture

Human T cell-derived cell lines [Jurkat, Hut78, MOLT4 (ATCC), MT-4, Jurkat-LTR-GFP (JLTRG), and PM1-CCR5 (NIH AIDS Reagent Program)] were used to obtain cell populations with chronic HIV-1 infection. Cells were cultured in RPMI 1640 medium (Sigma-Aldrich) supplemented with 10% fetal calf serum (Sigma-Aldrich), 50 U/mL penicillin, and 50 μg/mL kanamycin.

Drugs and reagents

The anti-HIV-1 reverse-transcriptase inhibitor EFdA/MK-8591/ISL was synthesized, as previously described (Nakata et al., 2007). The anti-HIV-1 protease inhibitor Darunavir (DRV) and the HIV-1 integrase inhibitor Dolutegravir (DTG) were purchased from Selleck (Houston, TX). PEP005 (PKC activator) was purchased from Cayman Chemical (Ann Arbor, MI); SAHA (vorinostat; HDAC inhibitor) from Santa Cruz Biotechnology (Dallas, TX); JQ-1 (BRD4 inhibitor) from BioVision (Milpitas, CA); GSK525762A (BRD4 inhibitor) from ChemScene (Monmouth Junction, NJ); Ro5-3335 from Merck (Darmstadt, Germany). Prostratin and Bryostatin-1 (PKC activator) were purchased from Sigma-Aldrich (St. Louis, MO), while Al-10-49 (CBFβ/RUNX inhibitor), Panobinostat (HDAC inhibitor), GS-9620 (TLR-7 agonist), and Birinapant (IAP inhibitor) were purchased from MedChem Express (Monmouth Junction, NJ). Phorbole 12-myristate13-acetate (PMA) and TNF-α were purchased from Wako Pure Chemical (Osaka, Japan) and BioLegend (San Diego, CA), respectively.

METHOD DETAILS

Establishment of the HIV-1 chronically infected cell culture model

Various T cell-derived cell lines [Jurkat, Hut78, MOLT4 (ATCC), MT-4, Jurkat-LTR-GFP (JLTRG), and PM1-CCR5 (NIH AIDS Reagent Program)] were used to obtain cell populations with chronic HIV-1 infection. Cells were infected with HIV-1_{NL4-3} or HIV-1_{JRFL} (PM1-CCR5) and cultured in RPMI 1640 medium (Sigma-Aldrich) supplemented with 10% fetal calf serum (Sigma-Aldrich), 50 U/mL penicillin, and 50 μg/mL kanamycin. Cells were passaged weekly to maintain cell numbers $<5 \times 10^6$ cells/mL when confluent. p24 levels in the supernatant were monitored using Lumipulse G1200 (FUJIREBIO, Tokyo, Japan). The number of cells with intracellular p24 was also monitored on day 30 after infection using flow cytometry (as described below).

HIV-1 reversal in latently infected cells and caspase-3 activation by LRAs

Chronically HIV-1_{NL4-3}-infected Jurkat/NL cells were treated with 1 of the 11 drugs (1 μM) for 24 h, after which changes in supernatant p24 levels and induction of caspase-3 activation were determined by flow cytometry.

Determination of antiviral activity of LRAs and conventional anti-HIV-1 drugs in Jurkat/NL cells (WIPE assay)

Jurkat/NL cells (5.0×10^4 cells/ml) were treated with a drug (e.g., EFdA, DRV, or PEP005) or a combination of drugs in a 12-well plate. Culture medium was exchanged, and the drug was added. Drug treatment was discontinued approximately on week 9 and the culture was maintained for an additional 8 weeks without drug supplementation. Supernatant p24 levels and intracellular HIV-1-DNA levels were monitored weekly during cell culture. At the end of each experiment, drug-treated cells with low/undetectable supernatant p24 levels were stimulated with 10 ng/mL TNF-α to confirm viral recurrence.

Flow cytometry analysis

The ratios of intracellular HIV-1 $p24^+$ cells, GFP^+ cells, and the active form of caspase-3 expression were determined as previously described (Hattori et al., 2018; Matsuda et al., 2019). Briefly, Jurkat/NL or JLTRG/NL cells were washed twice with phosphate buffered salts (PBS) and stained with Ghost Dye Red 780 (TONBO Biosciences, San Diego, CA) for 30 min at 4°C. The cells were then fixed with 1% paraformaldehyde/PBS for 20 min, and permeabilized in a flow cytometry perm buffer (TONBO Biosciences). After 5-min incubation at room temperature (25–30°C), cells were stained with anti-HIV-1 p24 (24-4)-fluorescein isothiocyanate (FITC) monoclonal antibody (mAb; Santa Cruz Biotechnology) and/or Alexafluor 647-conjugated anti-active caspase-3 mAb (C92-605; BD Pharmingen, San Diego, CA) for 30 min on ice. For propidium iodide (PI)/annexin V staining, cells were washed twice with PBS and resuspended in annexin V binding buffer (BioLegend) at a concentration of 1×10^7 cells/mL. The cells were then stained with FITC annexin V (BioLegend) and PI solution (BioLegend) for 15 min at room temperature. Cells were analyzed using a BD FACSVerse flow cytometer (BD Biosciences, Franklin Lakes, NJ). Data collected were analyzed using FlowJo software (Tree Star, Inc., Ashland, OR).

HIV-flow

The HIV-Flow assay (HIV double-staining) was used to quantify the cells expressing p24 protein upon TNF-α stimulation (Pardons et al., 2019). In brief, 5×10^5 Jurkat/NL cells were stimulated with 10 ng/mL TNF-α for 24 hrs. Following stimulation, cells were stained with Ghost Dye Violet 450 (TONBO Biosciences) for 30 min at 4°C. Then cells were fixed and permeabilized and stained with both anti-HIV-1 p24 -PE mAb (KC57) (Beckman Coulter) and anti-HIV-1 p24 -APC mAb (28B7) (MediMabs, Montreal, Canada) for 30 min at 4°C. Cells were washed twice by FACS buffer and analyzed using flow cytometry.

Sorting of GFP^+ or GFP^- cells from HIV-1_{NL4-3}-infected JLTRG cells

HIV-infected Jurkat-LTR-GFP cells (6×10^6) were resuspended in FACS buffer (PBS with 1% fetal calf serum), after which GFP^+ or GFP^- cells were sorted using BD FACS Aria I (BD Biosciences). The sorted GFP^- cells were stimulated with 10 ng/mL TNF-α for 6 h and then GFP expression levels were analyzed using BD FACSVerse (BD Biosciences). The level of *gag* expression after 18-h stimulation with 10 ng/mL TNF-α was analyzed by reverse-transcription (RT)-digital droplet PCR (ddPCR). ddPCR droplets were generated using the QX200 droplet generator (Bio-Rad Laboratories, Hercules, CA). RT-PCR was performed using a C1000 Touch thermal cycler (Bio-Rad Laboratories) with the primers listed in Table S2. The *gag*-positive and negative droplets were quantified based on fluorescence using the QX200 droplet reader (Bio-Rad Laboratories).

Isolation of PBMCs from HIV-1 infected individuals

Informed written consent was obtained from all participants (Table S1 Panel A) prior to the study. All subjects maintained low viral loads (<20 copies/mL; except for occasional blips) during therapy. $CD4^+$ T-cell counts in peripheral blood samples ranged from 447 to 632 cells/mm^3 (average 529 cells/mm^3). The plasma viral loads were <20 copies/mL, as determined using quantitative PCR (Roche COBAS AmpliPrep/COBAS TaqMan HIV-1 Test version 2.0) at the time of enrollment in the study. PBMCs were isolated from whole blood by density-gradient centrifugation using Ficoll-Paque (GE Healthcare, Chicago, IL). Total cellular DNA was extracted and used in subsequent PCR experiments.

RT-qPCR for HIV-1 mRNA quantification

Total cellular RNA was extracted from Jurkat cells infected with HIV-1 using the RNeasy Mini Kit (Qiagen) according to manufacturer's instructions. cDNA was synthesized using the PrimeScript RT Master Mix (Takara Bio). RT-qPCR analysis of intracellular HIV-1 mRNA was performed using PowerUp SYBR Green Master Mix (Applied Biosystems, Foster City, CA). Primer sequences used for the detection of HIV-1-RNA and β-actin gene are listed in Table S2. To determine the reactivation of HIV-1 in Jurkat/NL cells, relative HIV-1-RNA expression levels were normalized to that of β-actin gene.

Amplification of near-full-length single HIV-1 genome and sequencing

Nearly full-length single HIV-1 genome PCR was performed as described previously (Imamichi et al., 2016) with minor modifications. Briefly, genomic DNA was diluted to the single-genome level based on ddPCR and Poisson distribution statistics. The resulting single genome was amplified using Takara Ex Taq hot start version (first-round amplification). PCR conditions for first-round amplification consisted of 95°C for 2 min; followed by 5 cycles of 95°C for 10 s, 66°C for 10 s, and 68°C for 7 min; 5 cycles of 95°C for 10s, 63°C for 10 s, and 68°C for 7 min; 5 cycles of 95°C for 10 s, 61°C for 10 s, and 68°C for 7 min; 15 cycles of 95°C for 10 s, 58°C for 10 s, and 68°C for 7 min; and finally, 68°C for 5 min. First-round PCR products were diluted 1:50 in PCR-grade water and 5 μL of the diluted mixture

was subjected to second-round amplification. PCR conditions for the second-round amplification were as follows, 95°C for 2 min; followed by 8 cycles of 95°C for 10 s, 68°C for 10 s, and 68°C for 7 min; 12 cycles of 95°C for 10 s, 65°C for 10 s, and 68°C for 7 min; and finally, 68°C for 5 min. Primer information is provided in Table S2. PCR products were then visualized by electrophoresis on a 1% agarose gel. Based on Poisson distribution, samples with $\leq$30% positive reactions were considered to contain a single HIV-1 genome and were selected for sequencing. Amplified PCR products of the selected samples were purified using a QIAquick PCR Purification Kit (Qiagen) according to manufacturer's instructions. Purified PCR products were sheared by sonication using a Picoruptor device (Diagenode, Liege, Belgium) to obtain fragments with an average size of 300–400 bp. Libraries for next-generation sequencing (NGS) were prepared using the NEBNext Ultra II DNA Library Prep Kit for Illumina (New England Biolabs, Ipwich, MA) according to manufacturer's instructions. Concentration of library DNA was determined using the Qubit dsDNA High Sensitivity Assay kit (Invitrogen, Carlsbad, CA). The libraries were subsequently pooled together, followed by quantification using the Agilent 2200 TapeStation and quantitative PCR (GenNext NGS Library Quantification kit; Toyobo, Osaka, Japan), and sequenced using the Illumina MiSeq platform (Illumina, San Diego, CA). The resulting short reads were cleaned using an in-house Perl script (kindly provided by Dr. Michi Miura, Imperial College London, UK), which extracts reads with a high index-read sequencing quality (Phred score > 20) in each position of an 8-bp index read. Next, adapter sequences from Read1 and Read2 were removed, followed by a cleaning step to remove reads that were too short or had a very low Phred score, as previously described (Satou et al., 2017). The clean sequencing reads were aligned with the NL4-3 reference genome (GenBank-M19921) using the BWA-MEM algorithm (Li and Durbin, 2009). Further data processing and cleanup, including the removal of reads with multiple alignments and duplicated reads, were performed using Samtools (Li and Durbin, 2009) and Picard (http://broadinstitute.github.io/picard/). The aligned reads were visualized using Integrative Genomics Viewer (Robinson et al., 2011), and consensus sequences were copied and aligned using MUSCLE (Edgar, 2004). NGS analyses of nearly full-length HIV-1 PCR products from PBMCs of HIV-1-infected individuals were conducted using MinION platform with Flow Cell R9.4.1 and Rapid Barcoding kit (Oxford Nanopore Technologies, Oxford, UK), according to manufacturer's instructions. Sequencing reads cleaned using EPI2ME software (Oxford Nanopore Technologies) were aligned and analyzed as described above.

Ligation-mediated PCR (LM-PCR)

Detection of HIV-1 ISs was performed using ligation-mediated PCR and high-throughput sequencing, as previously described (Satou et al., 2017; Katsuya et al., 2021) but with minor modifications. Briefly, cellular genomic DNA was sheared by sonication using the Picoruptor device to obtain fragments with an average size of 300–400 bp. DNA ends were repaired using the NEBNext Ultra II End Repair Kit (New England Biolabs) and a DNA linker (Satou et al., 2017) was added. The junction between the 3′LTR of HIV-1 and host genomic DNA was amplified using a primer targeting the 3′LTR and a primer targeting the linker (Satou et al., 2017). PCR amplicons were purified using the QIAquick PCR Purification Kit (Qiagen) according to manufacturer's instructions. This was followed by Ampure XP bead purification (Beckman Coulter). Purified PCR amplicons were quantified using Agilent 2200 TapeStation and quantitative PCR (GenNext NGS library quantification kit; Toyobo). LM-PCR libraries were sequenced using the Illumina MiSeq as paired-end reads, and the resulting FASTQ files were analyzed as previously described (Satou et al., 2017). A circos plot showing virus ISs in the Jurkat/NL4-3 model and different cell lines was constructed using the OmicCircos tool available as a package in R software (Hu et al., 2014).

PCR-based HIV-1 RT enzyme assay

HIV-1 RT activity of supernatant viruses from experiment 1 shown in Figure 3D (no drug, EFdA treatment and EFdA plus PEP005 treatment) on weeks 9 and 17, and HIV-$_{1NL4-3}^{WT}$ were determined using PCR-based HIV-1 RT enzyme assay (Yasutake et al., 2018). In brief, viral lysate was prepared by incubating the mixture containing cell-free viral supernatant and virus lysis buffer (25mM Tris-HCl (pH 7.4), 1mM $MgCl_2$, 1mM DTT and 0.5% Triton X-100 final concentrations) for 10 min at room temperature. RT reaction mixture containing the viral lysate, MuLV RT buffer (New England Biolabs), 1mM dNTPs (TaKaRa Bio), 4U RNase inhibitor (TaKaRa Bio), 500nM MS2 reverse primer and pre-heated (65°C, 5 min) MS2 RNA (Roche, Mannheim, Germany) was prepared. The following reactions were performed: 60 min at 37°C, 5 min at 95°C. The real-time PCR was performed with SYBR Green and MS2 primer set. RT activity was calculated using a standard curve with series of a dilution of commercially available recombinant HIV-1 RT (Bio Academia, Osaka, Japan).

Viral replication kinetics and drug susceptibility assay

The viral replication kinetics of supernatant viruses from experiment 1 (no drug and EFdA treatment) on week 17, and HIV-1_{NL4-3}^{WT} were determined as previously described (Yasutake et al., 2018). In brief, MT-4 cells (2×10^4 cells/mL) were infected with viruses and the p24 values in supernatants were determined on days 0, 3, 6, 10 and 12. Drug susceptivity of each viruses for EFdA were performed as previously described (Maeda et al., 2014). MT-4 cells were infected with viruses and plated into each well of a 96-well culture plate containing various concentrations of EFdA (0–50 nM). Following incubation for 7 days, the number of viable cells was determined by the Cell Counting Kit-8 (Dojindo, Kumamoto, Japan) and the magnitude of HIV-1 inhibition by EFdA was determined based on their inhibitory effects of virally-induced cytopathicity in MT-4 cells. The IC_{50} values were determined using comparison with no-virus control cultures.

Bioinformatic analysis

Bed files containing the IS information were generated from the analyzed exported files. Data on RefSeq genes were obtained using UCSC Genome Browser (https://genome.ucsc.edu/) and the positions of RefSeq genes were compared with those of IS using the R package hiAnnotator (http://github.com/malnirav/hiAnnotator).

Mathematical modeling

Quantification of cell growth and death

We estimated the growth kinetics of Jurkat cells using the following mathematical model:

$$\frac{dT(t)}{dt} = gT(t)\left(1 - \frac{T(t)}{K}\right)$$

where the variables $T(t)$ represents the numbers of uninfected target cells at time t, and the parameters g and K represent the growth rate and the carrying capacity of the cell culture well, respectively. Note that latently infected cells have the same growth kinetics due to the lack of intracellular viral replications attributed to inactivation. Nonlinear least-squares regression was performed to the time-course numbers of Jurkat cells. The fitted parameter values are listed in Table S1 Panel B and the model behavior using these best-fit parameter estimates is presented together with the data in Figure S6A.

In addition, to estimate the death rate of virus-producing infected cells, treatments with a combination of EFdA (50 nM), DTG (500 nM), DRV (500 nM) and AMD3100 (1 μM) were initiated after the virus infection reached at steady state, and time-course numbers of those cells was measured for 7 days. Since the drug combination inhibited *de novo* infection, the decay kinetics of the virus-producing cells is described by the following model:

$$\frac{dI(t)}{dt} = -dI(t)$$

where the $I(t)$ represents the numbers of virus-producing cells at time t, and the parameter d represents the death rate. The fitted parameter values are listed in Table S1 Panel B and the model behavior using these best-fit parameter estimates is presented together with the data in Figure S6B.

Mathematical model describing HIV-1 infection dynamics in WIPE assay

We here introduce an extended mathematical model considering reactivation of latent HIV-1 reservoirs for analyzing experimental data in the WIPE assay (Figure S6C) (Perelson, 2002; Perelson et al., 1997; Rong and Perelson, 2009);

$$\frac{dT(t)}{dt} = gT(t)\left(1 - \frac{N(t)}{K}\right) - \beta T(t)V(t) - d_pT(t),$$

$$\frac{dI(t)}{dt} = (1-\theta)\beta T(t)V(t) + \varepsilon aL(t) - (b + d + d_p)I(t),$$

$$\frac{dL(t)}{dt} = \theta\beta T(t)V(t) + gL(t)\left(1 - \frac{N(t)}{K}\right) + bI(t) - (\varepsilon a + d_p)L(t),$$

$$\frac{dV(t)}{dt} = pI(t) - d_pV,$$

where $T(t)$ is the numbers of uninfected target cells, $I(t)$ and $L(t)$ are the numbers of virus-producing and latently infected cells per ml of a culture (i.e., the total cells are $N(t) = T(t) + I(t) + L(t)$), respectively, and $V(t)$ is the viral load measured by the amount of HIV-1 p24 per ml of culture supernatant. The uninfected and latently infected cells grow at a rate g with the carrying capacity of K (the maximum number of cells in the cell culture flask). It is assumed that a fraction θ becomes latently infected cells, and $1 - \theta$ is virus-producing infected cells having death rate d, when HIV-1 infect the target cells at rate β. The latently infected cells are reactivated at rate a, then (re-)start virus production at rate p (implying only intact proviral DNA is assumed), while the virus-producing cells become latently infected cell at rate b. We also assume that EFdA completely inhibits *de novo* infection (100% inhibition rate, $\beta = 0$) and PEP005 enhances the reactivation rate to εa where ε>1. Note that d_p represent the removal of virus and of the cells due to the experimental passage, and we fixed $d_p = 0.428$. In our earlier work (Iwami et al., 2012, 2015), we have shown that the approximating punctual removal as a continuous exponential decay has minimal impact on the model parameters and provides an appropriate fit to the experimental data.

Data fitting and parameter estimation

The parameters g, K and d were separately estimated, as discussed above, and fixed at 0.708 per day, 4.10×10^6 cells and 0.377 per day in Table S1 Panel B, respectively. A statistical model adopted from Bayesian inference assumed that measurement error followed

a normal distribution with mean zero and constant variance (error variance). The non-informative prior distributions with upper and lower limits were used as the prior distributions of parameters. The posterior predictive parameter distribution as an output of MCMC computation represented parameter variability. To analyze our cell culture experimental datasets, we simultaneously fitted $T(t) + L(t)$, $I(t)$, $V(t)$ and $(I(t) + L(t))/\{I(2\ \text{week}) + L(2\ \text{week})\}$ to the time-course of numbers of uninfected and latently infected (i.e., p24-negative) cells (cells/ml), virus producing (i.e., p24-positive) cells (cells/ml), supernatant p24 (pg/ml), and normalized proviral DNA at week 2 (first measurement in our experiments) without and with the antiviral drug(s) (Figure 6A). Distribution of model parameters (i.e., β, θ, a, b, p, and ε) along with initial values for variables ($T(0)$, $I(0)$, $L(0)$, and $V(0)$) were inferred directly by MCMC computations. The estimated parameters and initial values are listed in Table S1 Panel C and Panel D. Technical details of MCMC computations are summarized below.

QUANTIFICATION AND STATISTICAL ANALYSIS

For quantification of intracellular HIV-1 DNA levels, Total cellular DNA was extracted from cells (cell lines or PBMCs) using a QIAmp DNA Blood mini kit (Qiagen, Hilden, Germany) according to manufacturer's instructions. Quantitative PCR (qPCR) analysis of intracellular HIV-1 DNA levels was conducted using Premix Ex Taq (Probe qPCR) Rox plus (Takara Bio, Kusatsu, Japan). The oligonucleotides HIV-1 LTR and β2-microglobulin were used for HIV-1 DNA quantification and cell number determination, respectively (primer sequences are provided in Table S2 (Butler et al., 2001; Lee et al., 2017; Satou et al., 2017). HIV-1 proviral DNA copy and cell numbers were calculated based on a standard curve generated using a serially diluted pNL4-3 plasmid and DNA extracted from Jurkat cells, respectively.

Data analysis were performed using Prism 8 software (GraphPad Software, Inc., La Jolla, CA), unless otherwise stated. Differences between groups were analyzed for statistical significance using the Mann-Whitney U test and log-rank test. Statistical significance was defined as $P < 0.05$. Statistical analysis in mathematical models is described below. Package FME (Soetaert and Petzoldt, 2010) in R Statistical Software (R Core Team, 2019) was used to infer posterior predictive parameter distributions. The delayed rejection and Metropolis method (Haario et al., 2006) was used as a default computation scheme for FME to perform MCMC computations. MCMC computations for parameter inference were implemented using the pre-defined function modMCMC in package FME. Convergence of Markov chains to a stationary distribution was required to ensure parameter sets were sampled from a posterior distribution. Only the last 90,000 of 100,000 chains were used as burn-in. The convergence of the last 90,000 chains was manually checked with figures produced by package coda (Plummer et al., 2006), a collection of diagnostic tools for MCMC computation. The 95% credible interval shown as a shadowed region in each panel of Figure 6A was produced from 100 randomly chosen inferred parameter sets and corresponding model predictions. We used a bootstrap t-test (Efron and Tibshirani, 1994) to quantitatively characterize differences in derived quantities with and without antiviral drug (Figure 6B). In total, 100,000 parameter sets were sampled with replacement from the posterior predictive distributions to calculate the bootstrap t-statistics. To avoid potential sampling bias, the bootstrap t-test was performed 100 times repeatedly. The averages of the computed *p-value*s were used as indicators of differences.